

ABSTRACT

Remotely Sensed Hyperspectral Image Unmixing

Zhuocheng Yang, M.S.E.C.E.

Advisor: James B. Farison, Ph.D.

Estimating abundance fractions of materials in hyperspectral images is an important area of study in the field of remote sensing. The need for linear unmixing in remotely sensed imagery arises from the fact that the sampling distance is generally larger than the size of the targets of interest. We present two new unmixing methods, both of which are based on a linear mixture model. The first method requires two physical constraints imposed on abundance fractions: the abundance sum-to-one constraint and the abundance nonnegativity constraint. The second method relaxes the abundance sum-to-one constraint as this condition is rarely satisfied in reality and uses the relaxed sum-to-one constraint instead. Another contribution of this work is that the estimation is, unlike many other proposed methods, performed on noise reduced hyperspectral images instead of original images.

Remotely Sensed Hyperspectral Image Unmixing

by

Zhuocheng Yang, B.S.

A Thesis

Approved by the Department of Electrical and Computer Engineering

Kwang Y. Lee, Ph.D., Chairperson

Submitted to the Graduate Faculty of
Baylor University in Partial Fulfillment of the
Requirements for the Degree
of
Master of Science in Electrical and Computer Engineering

Approved by the Thesis Committee

James B. Farison, Ph.D., Chairperson

Michael W. Thompson, Ph.D.

Eunjee Song, Ph.D.

Accepted by the Graduate School
August 2010

J. Larry Lyon, Ph.D., Dean

Copyright © 2010 by Zhuocheng Yang

All rights reserved

TABLE OF CONTENTS

LIST OF ALGORITHMS	v
LIST OF FIGURES	vi
LIST OF TABLES	vii
ACRONYMS	viii
ACKNOWLEDGMENTS	x
DEDICATION	xi
CHAPTER ONE	1
Introduction	1
Hyperspectral Imagery	1
Linear Unmixing	3
Purpose and Overview of Thesis Research	3
CHAPTER TWO	5
Problem Formulation and Related Work	5
Linear Model	5
Problem Formulation	6
Related Work	6
Unconstrained Least Squares Estimation	9
Sum-to-One Constrained Least Squares Estimation	9
Fully Constrained Least Squares Linear Unmixing	10
CHAPTER THREE	12
Methods	12
Overview of Methods	12
Quadratic Programming Based Fully Constrained Least Squares	12
Noise-Adjusted Principal Components Transform Noise Reduction	16
Unmixing with Nonnegativity and Relaxed Sum-to-One Constraints	18
CHAPTER FOUR	22
Results	22
Simulations for Fully Constrained Least Squares	22
Real Hyperspectral Image Experiments for Fully Constrained Least Squares	30
Simulations for Unmixing with Nonnegativity and Relaxed Sum-to-One Constraints	39

CHAPTER FIVE	44
Conclusion and Future Work	44
Conclusion	44
Future Work	45
BIBLIOGRAPHY	46

LIST OF ALGORITHMS

Algorithm 3.1: QPFCLS Algorithm with SC and NC Constraints	15
Algorithm 3.2: R-QPFCLS Algorithm with RSC and NC Constraints	20

LIST OF FIGURES

Figure 1: An Example of a Hyperspectral Image [1]	1
Figure 2: Reflectance Spectrum of the Leaves of a Maple Tree	2
Figure 3: Simplified Procedure for Linear Unmixing [2]	3
Figure 4: Function $b(x)$ for Several Values of t	14
Figure 5: Illustration of the Linear Model [22]	19
Figure 6: Reflectance Spectra	22
Figure 7: Simulated Fractions	23
Figure 8: Estimation Results of (a) OSP, (b) SCLS, (c) FCLSLU, and (d) QPFCLS (SNR=30:1)	24
Figure 9: Estimation Results of (a) OSP, (b) SCLS, (c) FCLSLU, and (d) QPFCLS (SNR=10:1)	26
Figure 10: Estimation Results of (a) QPFCLS and QPFCLS with (b) 7, (c) 9, and (d) 15 PCs Reconstruction (SNR=10:1)	29
Figure 11: Spectral Band 30 of a Subimage of the AVIRIS Cuprite Image Scene	30
Figure 12: Spatial Locations of 22 Endmembers	31
Figure 13: 22 Fraction Images Obtained by OSP	35
Figure 14: 22 Fraction Images Obtained by QPFCLS with Noise Reduction	39
Figure 15: Estimation Results of (a) OSP, (b) SCLS, (c) QPFCLS, and (d) R-QPFCLS When Sum-to-One Condition Satisfied	41
Figure 16: Estimation Results of (a) OSP, (b) SCLS, (c) QPFCLS, and (d) R-QPFCLS When Sum-to-One Condition Not Satisfied	43

LIST OF TABLES

Table 1: Parameters for QPFCLS	25
Table 2: Root Mean Square Errors of Seven Materials (SNR=30:1)	25
Table 3: Root Mean Square Errors of Seven Materials (SNR=10:1)	27
Table 4: Root Mean Square Errors of Seven Materials with Noise Reduction (SNR=10:1)	28
Table 5: Parameters for R-QPFCLS	40
Table 6: Root Mean Square Errors of Seven Materials When Sum-to-One Condition Satisfied	42
Table 7: Root Mean Square Errors of Seven Materials When Sum-to-One Condition Not Satisfied	42

ACRONYMS

AVIRIS – Airborne Visible/Infrared Imaging Spectrometer

FCLSLU – Fully Constrained Least Squares Linear Unmixing

MNF – Maximum Noise Fraction

NAPC – Noise Adjusted Principal Components

NASA – National Aeronautics and Space Administration

NC – Nonnegativity Constraint

NCLS – Nonnegativity Constrained Least Squares

NNLS – Nonnegative Least Squares

OSP – Orthogonal Subspace Projection

PC – Principal Component

PCA – Principal Components Analysis

QP – Quadratic Programming

QPFCLS – Quadratic Programming Based Fully Constrained Least Squares

RMS – Root Mean Square

RSC – Relaxed Sum-to-One Constraint

R-QPFCLS – Relaxed-Quadratic Programming Based Fully Constrained Least Squares

SC – Sum-to-One Constraint

SCLS – Sum-to-One Constrained Least Squares

SD – Simultaneous Diagonalization

SNR – Signal-to-Noise Ratio

USGS – U.S. Geological Survey

ACKNOWLEDGMENTS

I would like to thank Dr. Farison for introducing me to the research area of hyperspectral imagery and for patient guidance and encouragement throughout my thesis work. I would like to thank Dr. Thompson for offering me the independent study to help me prepare my thesis work. And lastly, I would like to thank Baylor University School of Engineering and Computer Science for having me here.

DEDICATION

To my parents

CHAPTER ONE

Introduction

Hyperspectral Imagery

Hyperspectral imagery is an important technology often adopted in the field of remote sensing to collect detailed information about the material properties in a scene. The “hyper” in hyperspectral means that the images are simultaneously obtained in hundreds of narrow and contiguous bands, with wavelengths ranging from visible light to infrared bands. As a result, hyperspectral images offer more accurate and subtle information than any other type of remotely sensed data. Hyperspectral images are 3-dimensional arrays with two spatial dimensions and one spectral dimension. An example of a hyperspectral image is displayed in Figure 1. The image cube contains hundreds of

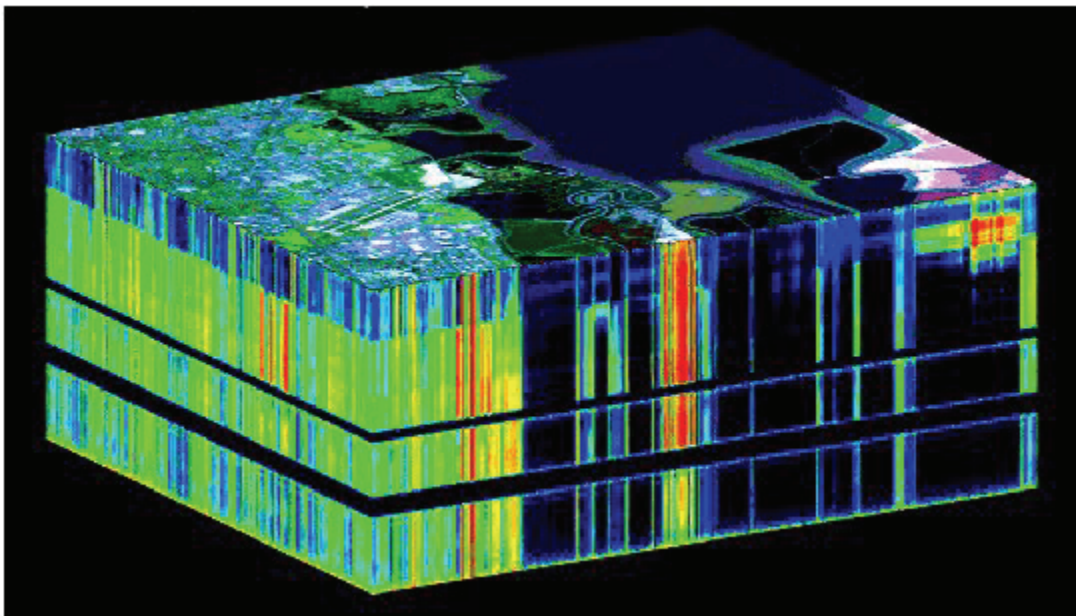


Figure 1: An Example of a Hyperspectral Image [1]

layers, with each layer obtained at a certain wavelength. A pixel in a hyperspectral image contains a vector which is the measure of the reflectance spectrum of that pixel area. The reflectance spectrum of a material is a plot of the ratio of reflected energy to incident energy as a function of wavelength. The reflectance spectrum of the leaves of a maple tree is illustrated in Figure 2. The shape of each reflectance curve varies from material to material, so the unique spectral information can be used to identify and discriminate different materials.

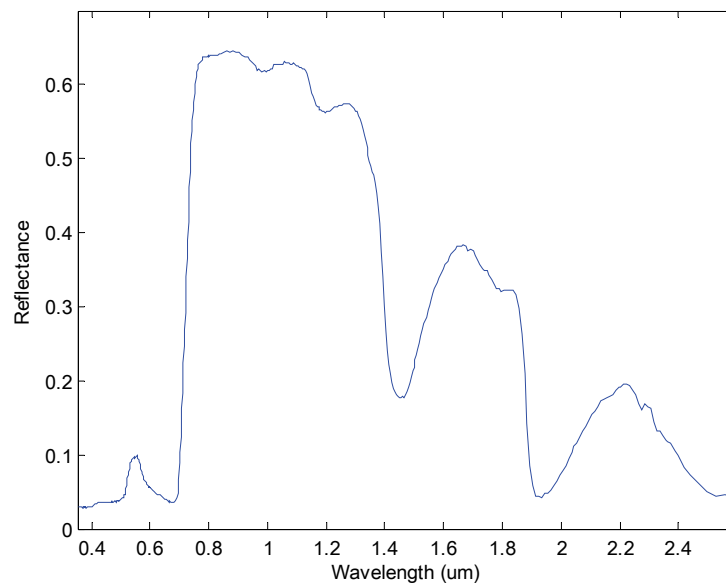


Figure 2: Reflectance Spectrum of the Leaves of a Maple Tree

Despite the fine spectral resolution, the underlying difficulty of studying hyperspectral images is due to the fact that the sampling distance is generally larger than the size of the targets of interest because hyperspectral sensing platforms usually fly at a high altitude. For example, NASA's Airborne Visible/Infrared Imaging Spectrometer (AVIRIS) has a spatial resolution of 20 meters when flying at 20 kilometers above sea

level. Under this circumstance, it is likely that a pixel area is occupied by more than one material and that the measured spectrum is actually a mixture of different material spectra. The fact that hyperspectral pixels of interest are frequently a combination of distinct material classes introduces a need to unmix these mixtures.

Linear Unmixing

Linear unmixing is the procedure by which the measured spectrum of a pixel is decomposed into a collection of material spectra, called endmembers, and the corresponding fractions that indicate the proportion of each endmember present in the pixel area. The procedure can be illustrated by Figure 3. The results of linear unmixing include one abundance fractional image for each endmember.

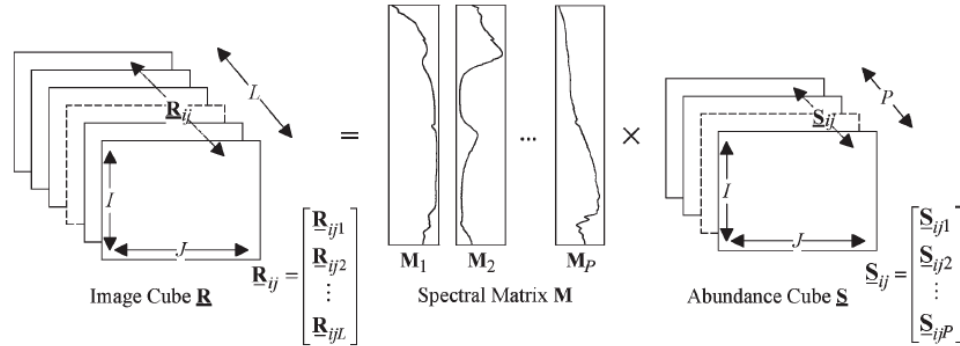


Figure 3: Simplified Procedure for Linear Unmixing [2]

Purpose and Overview of Thesis Research

The purpose of this research is to develop algorithms to automatically estimate endmember fractions via quadratic programming. To further enhance the performance of this approach, the noise adjusted principal components (NAPC) transform [3] is also used

to reduce the noise. Then, unlike many other methods, fraction estimation is performed on noise reduced hyperspectral images.

The remaining chapters in this thesis are organized as follows. Chapter Two provides an introduction to the linear model adopted in this thesis and the related work that has been developed in the last decade. Two least squares estimation methods based on quadratic programming and the noise reduction by the NAPC transform are described in Chapter Three. Computer simulations and real hyperspectral image experiments are demonstrated in Chapter Four to compare the performance of our methods with algorithms developed by others. Finally, a brief conclusion and suggestion for future work are offered in Chapter Five.

CHAPTER TWO

Problem Formulation and Related Work

Linear Model

Mathematical models for the mixing of different spectra provide the foundation for developing techniques to estimate the abundance fraction of each material from mixed pixels. Two mixture models have been proposed to represent the synthesis of the mixed pixels. One is a linear model that considers a mixed spectrum as a linear combination of endmember spectra present in the pixel area weighted by fractional area coverage [4]. The other model, suggested by Hapke, is a nonlinear model [5]. As the linear model is the most frequently used model for studying hyperspectral images, only the linear model is considered in this work.

For the sake of simplicity, we use the following notations throughout this thesis. Matrices are denoted using italic letters. Vectors are denoted using bold italic letters. Assume that the imaging system has L channels, each measuring the reflectance of one of the L spectral bands and that \mathbf{r} is an L -dimensional pixel vector containing the measured spectrum. Suppose that there are p ($p < L$) distinct endmembers present in the pixel area and their spectra are $\mathbf{m}_1, \mathbf{m}_2, \dots, \mathbf{m}_p$, respectively. The fraction α_i of each endmember is specified by the values $\alpha_1, \alpha_2, \dots, \alpha_p$. Then, the linear mixture model can be expressed as follows:

$$\mathbf{r} = \sum_i^p \alpha_i \mathbf{m}_i + \mathbf{n} \quad (2.1)$$

where \mathbf{n} represents additive noise. Equation (2.1) can also be written in the matrix form:

$$\mathbf{r} = M\boldsymbol{\alpha} + \mathbf{n} \quad (2.2)$$

where $M = [\mathbf{m}_1, \mathbf{m}_2, \dots, \mathbf{m}_p]$ and $\boldsymbol{\alpha} = [\alpha_1, \alpha_2, \dots, \alpha_p]$.

This linear model is subject to two constraints imposed on the fraction vector $\boldsymbol{\alpha}$. To be physically meaningful, the abundance nonnegativity constraint requires that all abundance fractions are nonnegative, such that $\alpha_i \geq 0$ for all $1 \leq i \leq p$. The abundance sum-to-one constraint demands that fractions in each pixel sum to one, such that $\sum_{i=1}^p \alpha_i = 1$. The inversion of Equation (2.2) is known as linear unmixing. Finding an accurate estimate of the vector $\boldsymbol{\alpha}$ is the primary goal of this work.

Problem Formulation

Considering the least squares error as the criterion for optimality, the linear unmixing can be formulated as the following optimization problem:

$$\text{Minimize } f(\boldsymbol{\alpha}) = (\mathbf{r} - M\boldsymbol{\alpha})^T (\mathbf{r} - M\boldsymbol{\alpha}) \quad (2.3)$$

subject to the sum-to-one constraint (SC) and the nonnegativity constraint (NC), expressed as follows:

$$\text{SC: } \mathbf{E}\boldsymbol{\alpha} = 1 \quad (2.4)$$

$$\text{NC: } \alpha_i \geq 0 \quad \forall 1 \leq i \leq p \quad (2.5)$$

where the p -dimensional vector $\mathbf{E} = [1, 1, \dots, 1]$.

Related Work

In order to estimate the desired target abundance fraction, Miller *et al.* proposed the simultaneous diagonalization (SD) filter [6], which gives an integrated filter

composed of an orthogonal operator and a matched filter. A subsequently similar approach named the orthogonal subspace projection (OSP) operator was suggested by Harsanyi and Chang [7] and later restudied by Chang [8]. The idea of these two approaches is to further decompose Equation (2.2) as follows:

$$\mathbf{r} = \mathbf{d}\alpha_p + U\boldsymbol{\gamma} + \mathbf{n} \quad (2.6)$$

where \mathbf{d} is the spectrum vector of the desired feature and α_p is the corresponding fraction. Without loss of generality, the last column of M in Equation (2.2) is assumed to be the desired spectral signature \mathbf{d} . The remaining columns of M are the corresponding spectral signatures of the undesired features, denoted by $U = [\mathbf{m}_1, \mathbf{m}_2, \dots, \mathbf{m}_{p-1}]$, and $\boldsymbol{\gamma}$ is the fraction vector of the undesired features. The SD filter is obtained by maximizing the ratio of the energy of the desired feature to the energy of the undesired features as well as the noise energy. The OSP operator is an orthogonal operator that projects \mathbf{r} onto a subspace that is orthogonal to the subspace spanned by the columns of U , followed by a matched filter to maximize the signal to noise ratio.

Other papers considered this problem from the signal estimation viewpoint. They produced a complete vector estimate $\hat{\boldsymbol{\alpha}}$ of the fraction vector $\boldsymbol{\alpha}$ rather than only the fraction of the desired target. Maximum likelihood estimation [9], [10] and unconstrained least squares estimation [11] have been introduced to solve this problem. Given white Gaussian noise, these two estimation methods achieve the same results. Moreover, $\hat{\boldsymbol{\alpha}}$

produced by unconstrained least squares estimation can be decomposed as $\begin{bmatrix} \hat{\boldsymbol{\gamma}} \\ \hat{\alpha}_p \end{bmatrix}$, where

$\hat{\alpha}_p$ is the same as the estimate of the desired feature obtained by the OSP operator [8]

and $\hat{\boldsymbol{\gamma}}$ is the estimate of the remaining undesired features. Thus, the OSP operator can be

considered as the scalar version of the unconstrained least squares estimation. The advantage of a vector estimate over scalar estimates (OSP and SD) is that the former can estimate p fractions at one time. It is also worth noting that the least squares estimator is valid for Gaussian as well as non-Gaussian noise. Therefore, this investigation uses the least squares error as the criterion for optimality in developing a vector estimate.

According to the Cramer-Rao Lower Bound theory, there exists a lower bound on the variance of any unbiased estimator [12]. All of the aforementioned estimates achieve this lower bound, given white Gaussian noise. In other words, all of these methods produce the optimal estimates from the mathematical point of view. However, one common drawback of these methods is that they do not utilize the abundance sum-to-one and abundance nonnegativity constraints. There has been some recent work reported in the literature considering these two constraints. The sum-to-one constrained least squares (SCLS) estimation can be solved by the technology of Lagrangian multipliers [12], [13], but neither the nonnegativity constrained least squares estimation nor the fully constrained least squares estimation has an analytical solution. A nonnegative least squares (NNLS) problem was solved iteratively [14] and later employed to estimate endmember fractions in [15], [16], where the method was referred to as the nonnegatively constrained least squares method. A fully constrained least squares linear unmixing (FCLSLU) method was suggested by Chang *et al.* [17], which was an extended version of the NNLS suggested by Haskell and Hanson [18].

In the following sections, we will introduce several of the least squares estimation methods mentioned above.

Unconstrained Least Squares Estimation

Setting gradient of $f(\boldsymbol{\alpha})$ in Equation (2.3) with respect to $\boldsymbol{\alpha}$ equal to zero yields:

$$\begin{aligned} \frac{df(\boldsymbol{\alpha})}{d\boldsymbol{\alpha}} \Big|_{\hat{\boldsymbol{\alpha}}_{UCLS}} &= 0 \\ 2M^T M \hat{\boldsymbol{\alpha}}_{UCLS} - 2M^T \mathbf{r} &= 0 \end{aligned} \quad (2.7)$$

The unconstrained least squares estimation is obtained:

$$\hat{\boldsymbol{\alpha}}_{UCLS} = (M^T M)^{-1} M^T \mathbf{r} \quad (2.8)$$

Sum-to-One Constrained Least Squares Estimation

Least squares estimation with the sum-to-one constraint can be tackled using Lagrangian multipliers. The fraction estimation can be determined by minimizing:

$$\begin{aligned} f(\boldsymbol{\alpha}, \lambda) &= (\mathbf{r} - M\boldsymbol{\alpha})^T (\mathbf{r} - M\boldsymbol{\alpha}) + \lambda(\mathbf{E}\boldsymbol{\alpha} - 1) \\ &= \boldsymbol{\alpha}^T M^T M \boldsymbol{\alpha} - 2\mathbf{r}^T M \boldsymbol{\alpha} + \mathbf{r}^T \mathbf{r} + \lambda \mathbf{E} \boldsymbol{\alpha} - \lambda \end{aligned} \quad (2.9)$$

where λ is a scalar Lagrangian multiplier. Setting the gradient of $f(\boldsymbol{\alpha}, \lambda)$ with respect to $\boldsymbol{\alpha}$ equal to zero gives:

$$\begin{aligned} \frac{\partial f(\boldsymbol{\alpha}, \lambda)}{\partial \boldsymbol{\alpha}} \Big|_{\hat{\boldsymbol{\alpha}}_{SCLS}} &= 0 \\ 2M^T M \hat{\boldsymbol{\alpha}}_{SCLS} - 2M^T \mathbf{r} + \lambda \mathbf{E}^T &= 0 \end{aligned} \quad (2.10)$$

and

$$\begin{aligned} \hat{\boldsymbol{\alpha}}_{SCLS} &= (M^T M)^{-1} M^T \mathbf{r} - \frac{\lambda}{2} (M^T M)^{-1} \mathbf{E}^T \\ &= \hat{\boldsymbol{\alpha}}_{UCLS} - \frac{\lambda}{2} (M^T M)^{-1} \mathbf{E}^T \end{aligned} \quad (2.11)$$

Applying the sum-to-one constraint, we have:

$$\mathbf{E} \hat{\boldsymbol{\alpha}}_{SCLS} = \mathbf{E} \hat{\boldsymbol{\alpha}}_{UCLS} - \frac{\lambda}{2} \mathbf{E} (M^T M)^{-1} \mathbf{E}^T = 1 \quad (2.12)$$

So

$$\frac{\lambda}{2} = [\mathbf{E}(\mathbf{M}^T \mathbf{M})^{-1} \mathbf{E}^T]^{-1} (\mathbf{E} \hat{\boldsymbol{\alpha}}_{UCLS} - 1) \quad (2.13)$$

The sum-to-one constrained least squares (SCLS) estimation can be obtained by

substituting $\frac{\lambda}{2}$ into Equation (2.11)

$$\hat{\boldsymbol{\alpha}}_{SCLS} = (\mathbf{M}^T \mathbf{M})^{-1} \mathbf{M}^T \mathbf{r} - [\mathbf{E}(\mathbf{M}^T \mathbf{M})^{-1} \mathbf{E}^T]^{-1} (\mathbf{E} \hat{\boldsymbol{\alpha}}_{UCLS} - 1) (\mathbf{M}^T \mathbf{M})^{-1} \mathbf{E}^T \quad (2.14)$$

Fully Constrained Least Squares Linear Unmixing

A fully constrained least squares linear unmixing method (FCLSLU) is suggested in [17]. That paper first considered the nonnegativity constrained least squares (NCLS) problem, which only imposed the nonnegativity constraint. The estimate can be found by minimizing:

$$\begin{aligned} f(\boldsymbol{\alpha}, \boldsymbol{\lambda}) &= (\mathbf{r} - \mathbf{M}\boldsymbol{\alpha})^T (\mathbf{r} - \mathbf{M}\boldsymbol{\alpha}) + \boldsymbol{\lambda}^T (\boldsymbol{\alpha} - \mathbf{c}) \\ &= \boldsymbol{\alpha}^T \mathbf{M}^T \mathbf{M} \boldsymbol{\alpha} - 2\mathbf{r}^T \mathbf{M} \boldsymbol{\alpha} + \mathbf{r}^T \mathbf{r} + \boldsymbol{\lambda}^T \boldsymbol{\alpha} - \boldsymbol{\lambda}^T \mathbf{c} \end{aligned} \quad (2.15)$$

where \mathbf{c} is the p -dimensional positive constant vector defined as $\mathbf{c} = [c_1, c_2, \dots, c_p]^T$ and

$\boldsymbol{\lambda}$ is the Lagrange multiplier vector defined as $\boldsymbol{\lambda} = [\lambda_1, \lambda_2, \dots, \lambda_p]^T$. Setting the gradient of

$f(\boldsymbol{\alpha}, \boldsymbol{\lambda})$ with respect to $\boldsymbol{\alpha}$ equal to zero gives:

$$\begin{aligned} \frac{\partial f(\boldsymbol{\alpha}, \boldsymbol{\lambda})}{\partial \boldsymbol{\alpha}} \Big|_{\hat{\boldsymbol{\alpha}}_{NCLS}} &= 0 \\ 2\mathbf{M}^T \mathbf{M} \hat{\boldsymbol{\alpha}}_{NCLS} - 2\mathbf{M}^T \mathbf{r} + \boldsymbol{\lambda} &= 0 \end{aligned} \quad (2.16)$$

Equation (2.16) leads to the following two iterative equations:

$$\hat{\boldsymbol{\alpha}}_{NCLS} = (\mathbf{M}^T \mathbf{M})^{-1} \mathbf{M}^T \mathbf{r} - \frac{1}{2} (\mathbf{M}^T \mathbf{M})^{-1} \boldsymbol{\lambda} \quad (2.17)$$

$$\boldsymbol{\lambda} = 2M^T (\mathbf{r} - M\hat{\boldsymbol{\alpha}}_{NCLS}) \quad (2.18)$$

The solution to the NCLS problem can be obtained by iterating Equations (2.17) and (2.18).

To find the fully constrained estimate, the spectra matrix M is replaced by $\begin{bmatrix} \delta M \\ \mathbf{E} \end{bmatrix}$

and the pixel vector \mathbf{r} is replaced by $\begin{bmatrix} \delta \mathbf{r} \\ 1 \end{bmatrix}$. The FCLSLU solution can be derived from the solution of Equations (2.17) and (2.18) using the new spectra matrix and the pixel vector [17]. The parameter δ is a very small number to control the impact of the sum-to-one constraint on FCLSLU. The value of δ is set to 10^{-6} in [17].

CHAPTER THREE

Methods

Overview of Methods

In this chapter, we discuss in detail our new constrained methods based on quadratic programming. Least squares error is used as the criterion for optimality, as it is valid for Gaussian as well as non-Gaussian noise. In addition, a noise reduction method is suggested in this chapter, which can further enhance the capability of our methods when the noise level rises.

Quadratic Programming Based Fully Constrained Least Squares

Quadratic programming (QP) is a convex optimization problem of minimizing a quadratic function subject to equality and inequality constraints, which can be expressed in the form:

$$\text{Minimize } f(\mathbf{x}) = \frac{1}{2} \mathbf{x}^T \mathbf{Q} \mathbf{x} + \mathbf{C}^T \mathbf{x} \quad (3.1a)$$

$$\text{subject to } \mathbf{G} \mathbf{x} = \mathbf{d} \text{ and } \mathbf{H} \mathbf{x} \leq \mathbf{b} \quad (3.1b)$$

We use this QP technology to achieve the fully constrained estimation. The method is referred to as quadratic programming based fully constrained least squares (QPFCLS) estimation. Before QP can be utilized, we first reorganize Equations (2.3)–(2.5) as follows:

$$\text{Minimize } f(\mathbf{a}) = \mathbf{a}^T \mathbf{M}^T \mathbf{M} \mathbf{a} - 2 \mathbf{r}^T \mathbf{M} \mathbf{a} + \mathbf{r}^T \mathbf{r} \quad (3.2a)$$

$$\text{subject to } \mathbf{E}\boldsymbol{\alpha} = 1 \text{ and } -\mathbf{B}\boldsymbol{\alpha} \leq \mathbf{0} \quad (3.2b)$$

where \mathbf{E} is a p -dimensional vector $[1, 1, \dots, 1]$ and \mathbf{B} is a $p \times p$ identity matrix. If we ignore the constant term $\mathbf{r}^T \mathbf{r}$, Equation (3.2a) is similar to (3.1a). The sum-to-one constraint is expressed as an equality constraint, while the nonnegativity constraint is replaced by an inequality constraint. The inequality symbol \leq in Equation (3.2b) represents componentwise inequality. Interior-point methods is capable of solving quadratic programming problems in practice [19]. The main idea behind the barrier method, a particular interior-point algorithm, is to put the inequality constraint into the objective function as follows:

$$\text{Minimize } f(\boldsymbol{\alpha}) = \boldsymbol{\alpha}^T \mathbf{M}^T \mathbf{M} \boldsymbol{\alpha} - 2\mathbf{r}^T \mathbf{M} \boldsymbol{\alpha} + \mathbf{r}^T \mathbf{r} + \sum_{i=1}^p h(-\mathbf{b}_i^T \boldsymbol{\alpha}) \quad (3.3a)$$

$$\text{subject to } \mathbf{E}\boldsymbol{\alpha} = 1 \quad (3.3b)$$

where \mathbf{b}_i^T is the i th row of \mathbf{B} and $h(x)$ is the indicator function defined as:

$$h(x) = \begin{cases} 0 & x \leq 0 \\ \infty & x > 0 \end{cases} \quad (3.4)$$

Violation of the nonnegativity constraint can lead to infinity in Equation (3.3a)

because $\sum_{i=1}^p h(-\mathbf{b}_i^T \boldsymbol{\alpha})$ approaches infinity, so minimizing Equation (3.3a) implicitly

guarantees that the nonnegativity constraint is satisfied. Since the function $\sum_{i=1}^p h(-\mathbf{b}_i^T \boldsymbol{\alpha})$

is not differentiable, the indicator function is approximated by the function $b(x)$ [19],

described as:

$$b(x) = -\frac{1}{t} \log(-x) \quad (3.5)$$

As t grows, the function $b(x)$ becomes a better approximation to $h(x)$ [19], and hence the estimation becomes more accurate. Figure 4 shows the function $b(x)$ for several values of t .

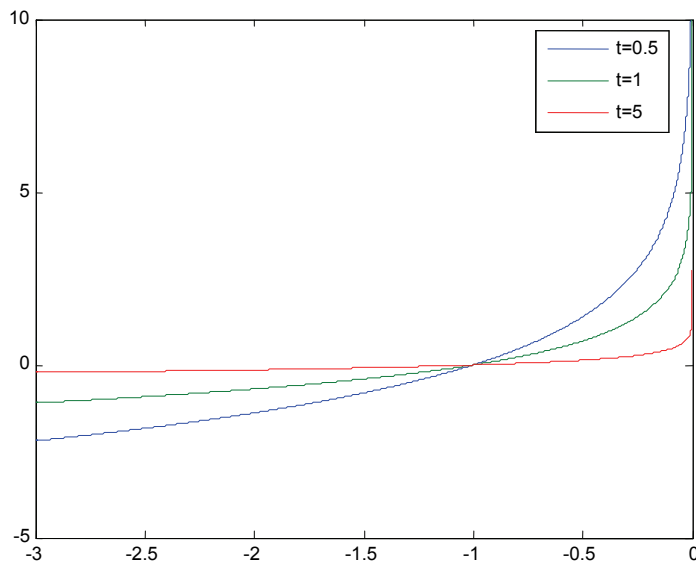


Figure 4: Function $b(x)$ for Several Values of t

Substituting $b(-\mathbf{b}_i^T \boldsymbol{\alpha})$ for $h(-\mathbf{b}_i^T \boldsymbol{\alpha})$ in Equation (3.3a) gives the final form:

$$\text{Minimize } f(\boldsymbol{\alpha}) = \boldsymbol{\alpha}^T \mathbf{M}^T \mathbf{M} \boldsymbol{\alpha} - 2\mathbf{r}^T \mathbf{M} \boldsymbol{\alpha} + \mathbf{r}^T \mathbf{r} + \sum_{i=1}^p -\frac{1}{t} \log(\mathbf{b}_i^T \boldsymbol{\alpha}) \quad (3.6a)$$

$$\text{subject to } \mathbf{E} \boldsymbol{\alpha} = 1 \quad (3.6b)$$

However, when the value of t is large, Equation (3.6) is difficult to minimize. To overcome this dilemma, the estimate $\hat{\boldsymbol{\alpha}}_{QPFLS}$ for the above optimization problem is obtained by repeatedly applying Newton's method to a sequence of equality constrained problems [19]. The value of t increases at each iteration until the stopping criterion is satisfied, and Newton's method is implemented to find an estimate from Equation (3.6). Then, this estimate is used as the starting point for the next iteration. A vector with equal

fractions is used as the initial starting point. The details of implementing the QPFCLS method are given in Algorithm 3.1.

Algorithm 3.1 QPFCLS Algorithm with SC and NC Constraints

```

1: Initialize parameters  $t, \alpha^{(1)}, \mu, \varepsilon, \varepsilon_{Newton}$ 
2:  $k = 1$ 
3: while  $p/t > \varepsilon$  do
4:   Compute the Newton step  $\Delta\alpha^{(k)}$  and the decrement  $\lambda$ 
5:   while  $\lambda > \varepsilon_{Newton}$  do
6:     Find step size  $\tau$  by backtracking line search
7:      $\alpha^{(k)} = \alpha^{(k)} + \tau\Delta\alpha^{(k)}$ 
8:     Compute the Newton step  $\Delta\alpha^{(k)}$  and the decrement  $\lambda$ 
9:   end while
10:   $t = \mu t$ 
11:   $\alpha^{(k+1)} = \alpha^{(k)}, k = k + 1$ 
12: end while
13:  $\hat{\alpha}_{QPFCLS} = \alpha^{(k)}$ 

```

The Newton step $\Delta\alpha^{(k)}$ is the solution of the following $p + 1$ linear equations:

$$\begin{bmatrix} \nabla^2 f(\alpha^{(k)}) & \mathbf{E}^T \\ \mathbf{E} & \mathbf{0} \end{bmatrix} \begin{bmatrix} \Delta\alpha^{(k)} \\ w \end{bmatrix} = \begin{bmatrix} -\nabla f(\alpha^{(k)}) \\ \mathbf{0} \end{bmatrix} \quad (3.7)$$

where $\nabla^2 f$ and ∇f are the first and second derivatives of function $f(\alpha)$, respectively.

Equation (3.7) guarantees that $\alpha^{(k)}$ moves along the descent direction, such that

$f(\alpha^{(k)}) > f(\alpha^{(k)} + \tau\Delta\alpha^{(k)})$ holds, and that the updated solution $\alpha^{(k)} + \tau\Delta\alpha^{(k)}$ is a feasible solution, such that $\mathbf{E}(\alpha^{(k)} + \tau\Delta\alpha^{(k)}) = \mathbf{1}$ holds as long as the starting point is feasible. The

Newton decrement λ determined by $[(\Delta\alpha^{(k)})^T \nabla^2 f(\alpha^{(k)}) \Delta\alpha^{(k)}]^{1/2}$ is used as the stopping criterion for the inner while loop. The number of the distinct endmembers is specified by the value of p .

Noise-Adjusted Principal Components Transform Noise Reduction

To further enhance the performance of our method, we use the noise-adjusted principal components (NAPC) transform [19], which is an extension of the principal components analysis (PCA), to reduce noise in hyperspectral images and perform the QPFCLS on noise reduced images. If the hyperspectral pixel vectors are considered as realizations of a random vector, the PCA finds linearly transformed data ordered by decreasing variance by the linear transformation:

$$\mathbf{r}_{PC} = A_{PC}^T \mathbf{r} \quad (3.8)$$

assuming the mean has been subtracted from the data. A_{PC} , the transform matrix, is the eigenvector matrix of the covariance matrix of \mathbf{r} . The covariance matrix of \mathbf{r}_{PC} is given by:

$$\Sigma_{PC} = E(\mathbf{r}_{PC} \mathbf{r}_{PC}^T) = E(A_{PC}^T \mathbf{r} \mathbf{r}^T A_{PC}) = A_{PC}^T E(\mathbf{r} \mathbf{r}^T) A_{PC} = \lambda_{\Sigma} \quad (3.9)$$

where E is the expectation. $E(\mathbf{r} \mathbf{r}^T)$ is actually the covariance matrix of \mathbf{r} since \mathbf{r} is zero mean. By eigendecomposition, we find that λ_{Σ} is the diagonal matrix whose diagonal elements are the eigenvalues of the covariance matrix of \mathbf{r} . We assume that the eigenvalues in λ_{Σ} are ordered by decreasing value. Notice that the transformed data are de-correlated and have decreasing data variance.

However, it is revealed that data variance does not necessarily reflect signal-to-noise ratio (SNR) if different bands have unequal noise variances [20], and thus a component with large variance does not necessarily indicate high SNR. To deal with this problem, Green *et al.* [20] proposed a maximum noise fraction (MNF) transform which can produce components ordered by decreasing SNR instead of variance as is used in the

PCA. The MNF transform was reinterpreted as the noise-adjusted principal components (NAPC) transform [19], which is a two-stage process. Image data are first whitened so that the noise covariance matrix becomes an identity matrix, and then the standard PCA is applied to the whitened image data. In this section we discuss how the NAPC can be used to reduce noise in hyperspectral images.

First, the noise covariance matrix Σ_n is obtained from prior knowledge or estimated directly from images. One particular method that will be used in this paper was suggested by Roger [21]. Then the orthonormal eigenvector matrix V and the diagonal matrix $\Delta\lambda$ of eigenvalues are computed. The whitening transform matrix is obtained by $F = V\Delta\lambda^{-\frac{1}{2}}$. Image data are whitened by transforming each pixel vector by:

$$\mathbf{r}_w = F\mathbf{r} \quad (3.10)$$

Then the covariance matrix of the whitened data, denoted by Σ_w , is calculated, and then the standard PCA is applied to obtain the eigenvector matrix A of Σ_w . Noise reduction can be achieved by deleting the noisiest components. Therefore, we only retain the first k eigenvectors in A , with the new matrix denoted by \hat{A} . The transformed data can be obtained by:

$$\mathbf{y} = \hat{A}^T(\mathbf{r}_w - \mathbf{m}_g) \quad (3.11)$$

where \mathbf{m}_g is the sample mean vector of the whitened image data. The reconstruction $\hat{\mathbf{r}}$ of \mathbf{r} can be determined by:

$$\hat{\mathbf{r}} = F^{-1}(\hat{A}\mathbf{y} + \mathbf{m}_g) \quad (3.12)$$

It is worth noting that if the additive noise is independent and identically distributed (i.i.d.), the NAPC transform is actually identical to the PCA. Another issue

encountered in this noise reduction method is the number of eigenvectors in A that should be retained. It turns out that this number is related to the number of distinct endmembers in image data. Suppose that hyperspectral images are generated from L spectral bands, and that there are p distinct endmembers. We should get p significant eigenvalues of Σ_w , and $L - p$ less significant eigenvalues. These significant eigenvalues contain most of the useful signals, while $L - p$ eigenvalues correspond to noisy components. Therefore, if we retain the first p eigenvectors in A , we find the optimal reconstruction \hat{r} . If the number of endmembers is known *a priori*, we should keep the same number of the eigenvectors in A . However, in most cases, when such knowledge is not accessible, we can still estimate the number of the endmembers directly from the image data. It is always safe to keep more eigenvectors than the estimated number of the endmembers, especially when such estimation becomes less reliable as the noise level rises. Experiments in the next chapter show that even though the performance of fraction estimation degrades slightly as more eigenvectors are retained, estimation results are still significantly improved.

Unmixing with Nonnegativity and Relaxed Sum-to-One Constraints

The linear mixture model has been a dominant model in the literature for the study of remotely sensed image data. It has been pointed out that the linear model implicitly suggests the sum-to-one constraint; that is, $\sum_{i=1}^p \alpha_i = 1$. Nevertheless, this constraint is strictly valid only for the situation where endmembers in a pixel are arranged on the surface in a segregated manner, analogous to the squares on a checkerboard [22], as depicted in Figure 5. In reality, however, endmembers are more or less distributed in a

homogeneous way, which makes the sum-to-one constraint not strictly valid. As a result, a method specifically designed for the sum-to-one constraint can easily become vulnerable when the sum-to-one condition is not met. In this section, we propose a relaxed sum-to-one constraint and develop a corresponding method for this relaxation. The sum of the estimated fractions in every pixel is bound to a range rather than being fixed on the value of one. From here on, we call this new constraint the relaxed sum-to-one constraint. The method with the relaxed sum-to-one and nonnegativity constraints is referred to as the relaxed-quadratic programming based fully constrained least squares (R-QPFCLS).

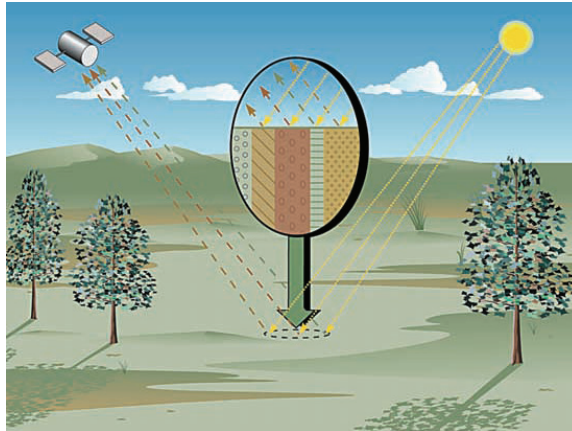


Figure 5: Illustration of the Linear Model [22]

The relaxed sum-to-one constraint (RSC) and the nonnegativity constraint (NC) have the following forms:

$$\text{RSC} : l \leq \mathbf{E}\mathbf{a} \leq h \quad (3.13)$$

$$\text{NC} : -\mathbf{B}\mathbf{a} \leq 0 \quad (3.14)$$

where the p -dimensional vector $\mathbf{E} = [1, 1, \dots, 1]$, \mathbf{B} is a $p \times p$ identity matrix, and p is the number of the endmembers present in the pixel area. The lower bound l and upper

bound h define the box constraint imposed on the abundance fractions. Combining

Equations (3.13) and (3.14), we get one inequality constraint $H\boldsymbol{\alpha} \leq \mathbf{q}$, where $H = \begin{bmatrix} -B \\ \mathbf{E} \\ -\mathbf{E} \end{bmatrix}$

and $\mathbf{q} = \begin{bmatrix} 0 \\ h \\ -l \end{bmatrix}$. The same barrier method discussed in the previous section can solve this

optimization problem, too. By putting the inequality constraint into the objective function

by the logarithmic barrier function $\sum_{i=1}^p -\frac{1}{t} \log(-\mathbf{H}_i^T \boldsymbol{\alpha} + q_i)$, where \mathbf{H}_i^T is the i th row of

H , the final form can be obtained as follows:

$$\text{Minimize } f(\boldsymbol{\alpha}) = \boldsymbol{\alpha}^T M^T M \boldsymbol{\alpha} - 2\mathbf{r}^T M \boldsymbol{\alpha} + \mathbf{r}^T \mathbf{r} + \sum_{i=1}^p -\frac{1}{t} \log(-\mathbf{H}_i^T \boldsymbol{\alpha} + q_i) \quad (3.15)$$

The discussion about t in Equation (3.6a) applies to (3.15), too. Newton's method repeatedly applied to a sequence of unconstrained problems can find an estimate for

Equation (3.15). The details of our method are given in Algorithm 3.2. The Newton step

$\Delta \boldsymbol{\alpha}^{(k)}$ and Newton decrement λ are determined by $-\nabla^2 f(\boldsymbol{\alpha}^{(k)})^{-1} \nabla f(\boldsymbol{\alpha}^{(k)})$ and

$\left[(\Delta \boldsymbol{\alpha}^{(k)})^T \nabla^2 f(\boldsymbol{\alpha}^{(k)}) \Delta \boldsymbol{\alpha}^{(k)} \right]^{\frac{1}{2}}$. As before, it is guaranteed that $\boldsymbol{\alpha}^{(k)}$ moves along the descent

direction.

Algorithm 3.2 R-QPFCLS Algorithm with RSC and NC Constraints

- 1: Initialize parameters $t, \boldsymbol{\alpha}^{(1)}, \boldsymbol{\mu}, \boldsymbol{\varepsilon}, \boldsymbol{\varepsilon}_{Newton}$
- 2: $k = 1$
- 3: **while** $p/t > \boldsymbol{\varepsilon}$ **do**
- 4: Compute the Newton step $\Delta \boldsymbol{\alpha}^{(k)}$ and the decrement λ
- 5: **while** $\lambda > \boldsymbol{\varepsilon}_{Newton}$ **do**
- 6: Find step size τ by backtracking line search
- 7: $\boldsymbol{\alpha}^{(k)} = \boldsymbol{\alpha}^{(k)} + \tau \Delta \boldsymbol{\alpha}^{(k)}$

8: Compute the Newton step $\Delta\boldsymbol{\alpha}^{(k)}$ and the decrement λ
9: **end while**
10: $t = \mu t$
11: $\boldsymbol{\alpha}^{(k+1)} = \boldsymbol{\alpha}^{(k)}, k = k + 1$
12: **end while**
13: $\hat{\boldsymbol{\alpha}}_{R-QPFCLS} = \boldsymbol{\alpha}^{(k)}$

CHAPTER FOUR

Results

Simulations for Fully Constrained Least Squares

Implemented without Noise Reduction

In this section, we demonstrate a comparative analysis among the OSP [7], SCLS, FCLSLU [16], and QPFCLS. A set of reflectance spectra is selected from the U.S. Geological Survey (USGS) Digital Spectral Library [23]. The set contains seven vegetation spectra: maple leaf, blackbrush, pinon pine, aspen leaf, saltbrush, azurite, and sagebrush. Their respective spectra are shown in Figure 6. Their fractions in each pixel

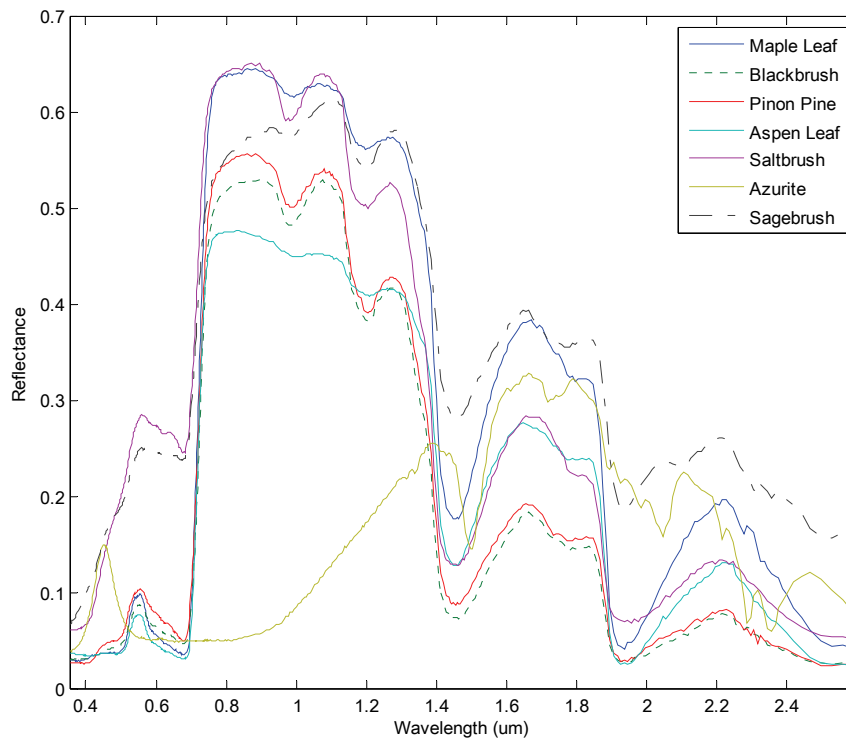


Figure 6: Reflectance Spectra

are illustrated in Figure 7. In this example, 1000 mixed pixels are simulated according to the linear model in Equation (2.2). The sum of the fractions in each pixel is set to one to comply with the sum-to-one constraint. White Gaussian noise is added to every spectral band to achieve the SNR of 30:1. The SNR is defined as $\frac{1}{L} \sum_{i=1}^L SNR_i$, where L is the number of the bands and SNR_i is the SNR of the i th band, defined as 50% of the averaged reflectance in the i th band divided by the standard deviation of the noise.

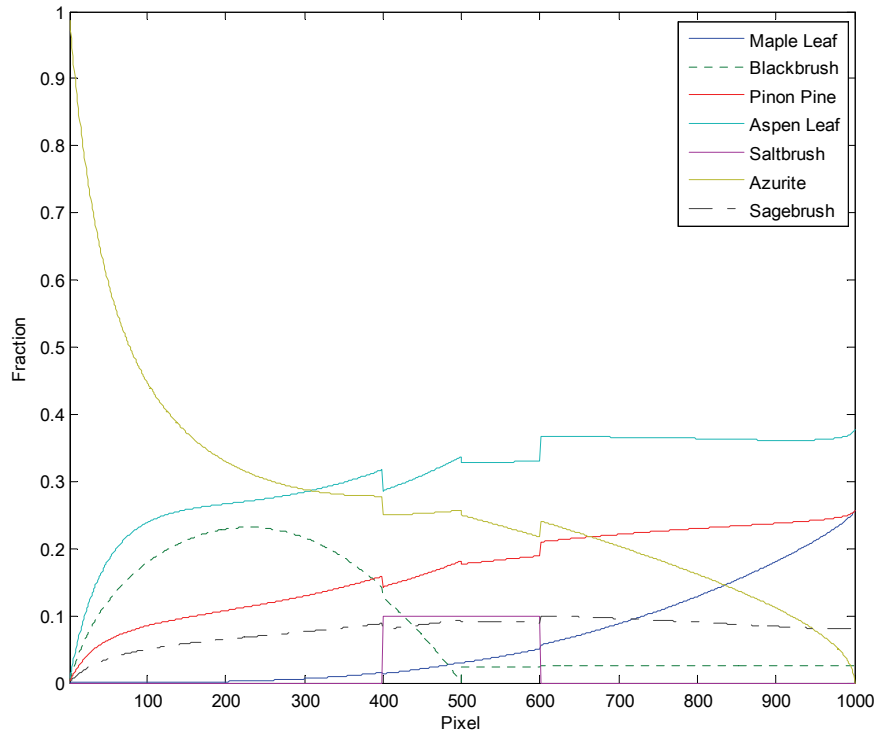


Figure 7: Simulated Fractions

Four methods, the OSP, SCLS, FCLSLU, and QPFCLS, are implemented to estimate the fraction of saltbrush, which is added only to pixel numbers 400–600 with

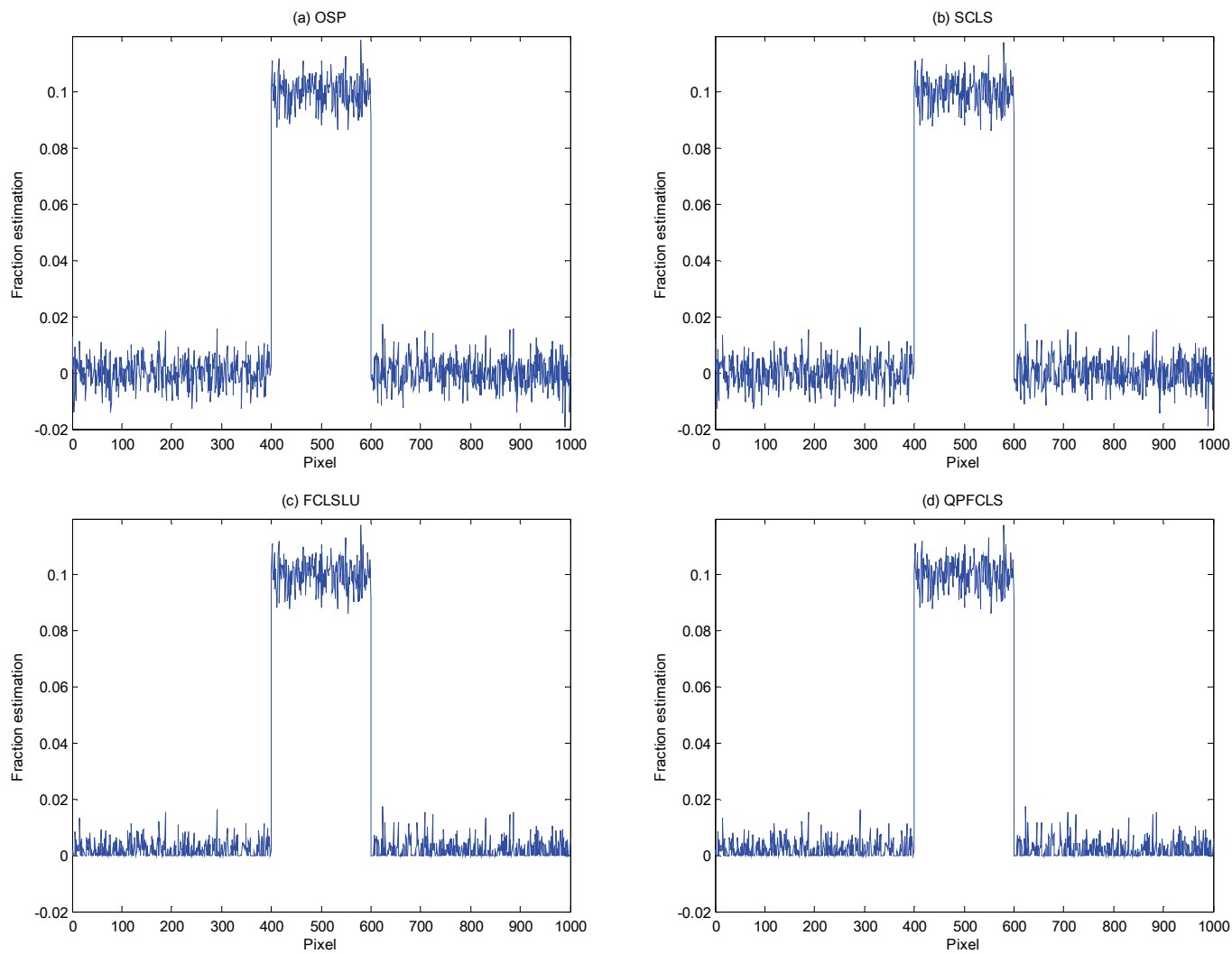


Figure 8: Estimation Results of (a) OSP, (b) SCLS, (c) FCLSLU, and (d) QPFCLS (SNR=30:1)

10% abundance fraction. Their resulting estimated fractions are displayed in Figure 8.

The parameters for the implementation of the QPFCLS are listed in Table 1.

Table 1: Parameters for QPFCLS

t	$\alpha^{(1)}$	μ	ε	ε_{Newton}
4000	Equal Fractions	50	1.0×10^{-5}	1.0×10^{-5}

We can see that the OSP and SCLS produce some negative fractions, which is physically meaningless. Two fully constrained methods, the FCLSLU and our method, QPFCLS, generate nonnegative results. To better compare the performance of each method, we calculate the root mean square (RMS) error between the actual and estimated fractions. The RMS errors are 5.344×10^{-3} for OSP, 5.273×10^{-3} for SCLS, 4.218×10^{-3} for FCLSLU, and 4.219×10^{-3} for QPFCLS. The RMS errors of all seven materials are listed in Table 2. The FCLSLU and QPFCLS produce the best estimates for all materials.

Table 2: Root Mean Square Errors of Seven Materials (SNR=30:1)

Endmember	OSP	SCLS	FCLSLU	QPFCLS
Maple leaf	1.455×10^{-2}	7.730×10^{-3}	6.787×10^{-3}	6.787×10^{-3}
Blackbrush	2.746×10^{-2}	2.462×10^{-2}	2.222×10^{-2}	2.222×10^{-2}
Pinon pine	3.022×10^{-2}	2.913×10^{-2}	2.603×10^{-2}	2.603×10^{-2}
Aspen leaf	1.928×10^{-2}	1.349×10^{-2}	1.261×10^{-2}	1.261×10^{-2}
Saltbrush	5.344×10^{-3}	5.273×10^{-3}	4.218×10^{-3}	4.219×10^{-3}
Azurite	4.401×10^{-3}	3.983×10^{-3}	3.567×10^{-3}	3.567×10^{-3}
Sagebrush	5.811×10^{-3}	5.807×10^{-3}	4.788×10^{-3}	4.788×10^{-3}

Next, the SNR is reduced to 10:1 in order to demonstrate the capability of each estimation approach at high noise level. The estimation results are shown in Figure 9. As SNR decreases, the estimation results degrade dramatically. Again, we find that both the

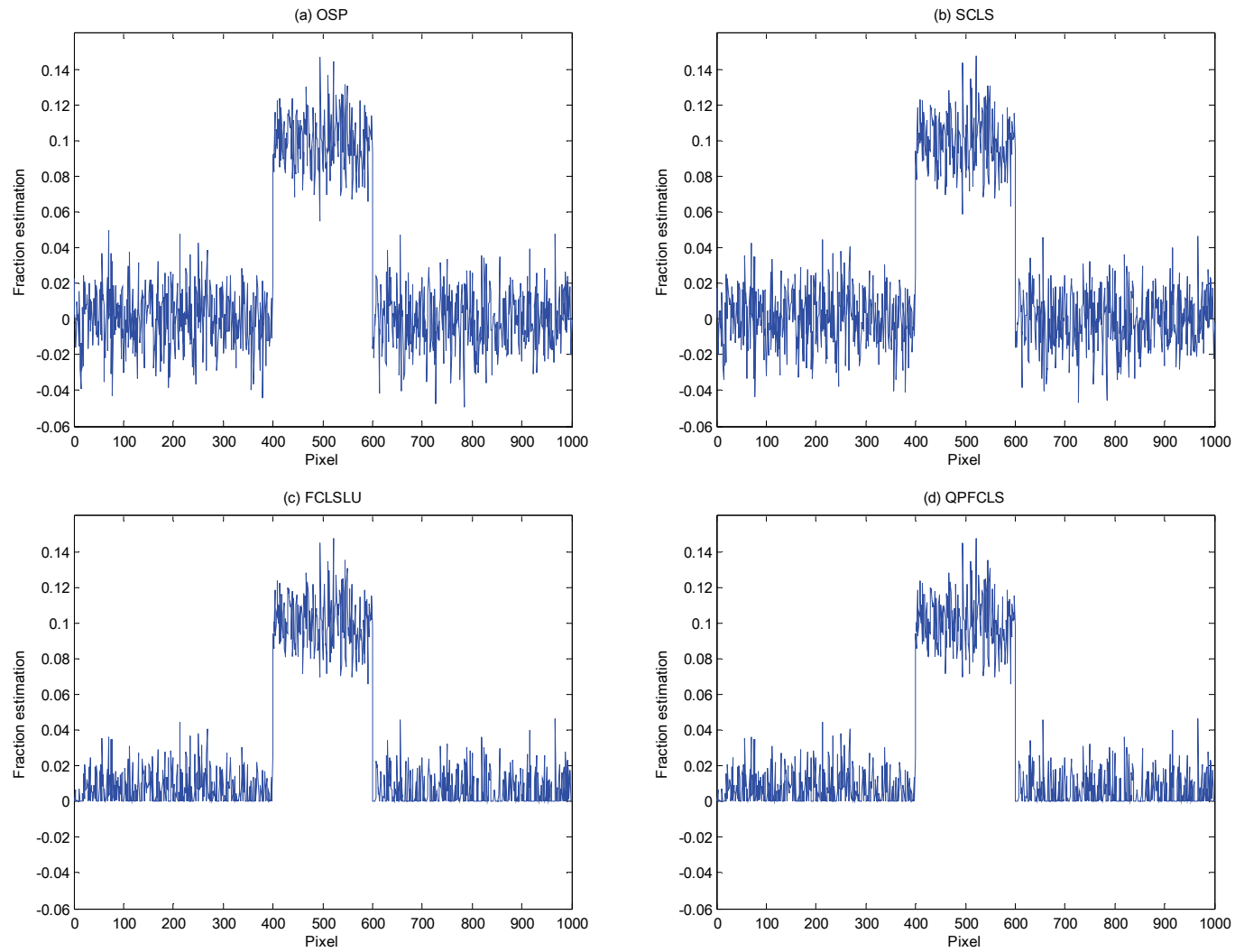


Figure 9: Estimation Results of (a) OSP, (b) SCLS, (c) FCLSLU, and (d) QPFCLS (SNR=10:1)

OSP and SCLS produce negative fractions. The RMS errors are 1.621×10^{-2} for OSP, 1.589×10^{-2} for SCLS, 1.228×10^{-2} for FCLSLU, and 1.227×10^{-2} for QPFCLS. The RMS errors of all seven materials are shown in Table 3. In both cases, we find that the FCLSLU and QPFCLS perform comparably while OSP always performs the worst. This is because the FCLSLU and QPFCLS apply both the sum-to-one and nonnegativity constraints, but OSP is just an unconstrained estimation approach. In addition, SCLS performs slightly better than OSP, which indicates that applying the sum-to-one constraint alone does not lead to a significant improvement in estimation performance.

Table 3: Root Mean Square Errors of Seven Materials (SNR=10:1)

Endmember	OSP	SCLS	FCLSLU	QPFCLS
Maple leaf	4.527×10^{-2}	2.292×10^{-2}	1.917×10^{-2}	1.917×10^{-2}
Blackbrush	8.292×10^{-2}	7.473×10^{-2}	6.022×10^{-2}	6.016×10^{-2}
Pinon pine	9.158×10^{-2}	8.859×10^{-2}	7.152×10^{-2}	7.145×10^{-2}
Aspen leaf	5.922×10^{-2}	4.003×10^{-2}	3.578×10^{-2}	3.578×10^{-2}
Saltbrush	1.621×10^{-2}	1.589×10^{-2}	1.228×10^{-2}	1.227×10^{-2}
Azurite	1.308×10^{-2}	1.189×10^{-2}	9.930×10^{-3}	9.931×10^{-3}
Sagebrush	1.767×10^{-2}	1.768×10^{-2}	1.385×10^{-2}	1.385×10^{-2}

Implemented with Noise Reduction

We have demonstrated that as noise level rises, the estimation results degrade. We will show in this example that noise reduction can noticeably enhance the estimation performance. The same reflectance spectra and simulated fractions are used here. White Gaussian noise is added to achieve the SNR of 10:1. Because we attempt to demonstrate the effectiveness of noise reduction, only the QPFCLS is considered in this example. The QPFCLS implemented with the same parameters as in Table 1 is performed on the noise reduced images instead of the original images. The number of the endmembers is

assumed to be known. Estimation results from images reconstructed from 7, 9, and 15 principal components (PCs), respectively, are displayed in Figure 10. The fraction estimation obtained by the QPFCLS without noise reduction is also included for better comparison. The RMS errors are 8.129×10^{-3} for 7 PCs, 8.288×10^{-3} for 9 PCs, and 8.539×10^{-3} for 15 PCs. Recall that the RMS error is 1.227×10^{-2} for QPFCLS from the previous example. The RMS errors of all seven materials are shown in Table 4. It can be observed from this example that even though the performance of fraction estimation deteriorates slightly as more PCs are included for reconstruction, the estimation results are still much better than those generated by the QPFCLS without noise reduction.

Table 4: Root Mean Square Errors of Seven Materials with Noise Reduction (SNR=10:1)

Endmember	QPFCLS	QPFCLS-7 PCs	QPFCLS-9 PCs	QPFCLS-15 PCs
Maple leaf	1.917×10^{-2}	1.472×10^{-2}	1.482×10^{-2}	1.535×10^{-2}
Blackbrush	6.016×10^{-2}	1.922×10^{-2}	1.943×10^{-2}	2.471×10^{-2}
Pinon pine	7.145×10^{-2}	1.761×10^{-2}	1.787×10^{-2}	2.727×10^{-2}
Aspen leaf	3.578×10^{-2}	2.068×10^{-2}	2.068×10^{-2}	2.321×10^{-2}
Saltbrush	1.227×10^{-2}	8.129×10^{-3}	8.288×10^{-3}	8.539×10^{-3}
Azurite	9.931×10^{-3}	6.420×10^{-3}	6.457×10^{-3}	6.994×10^{-3}
Sagebrush	1.385×10^{-2}	8.847×10^{-3}	9.049×10^{-3}	9.239×10^{-3}

When the number of the endmembers is not accessible, a Neyman-Pearson detection theory-based thresholding method proposed by [24] can be used to estimate this number. By setting the false-alarm probability to 10^{-4} , this method leads to an estimate of the number of the endmembers equal to 4 as opposed to 7 material spectra used in this example. It is our belief that it may be a good practice to use more PCs than the estimated number of materials because it becomes more complicated to accurately estimate this

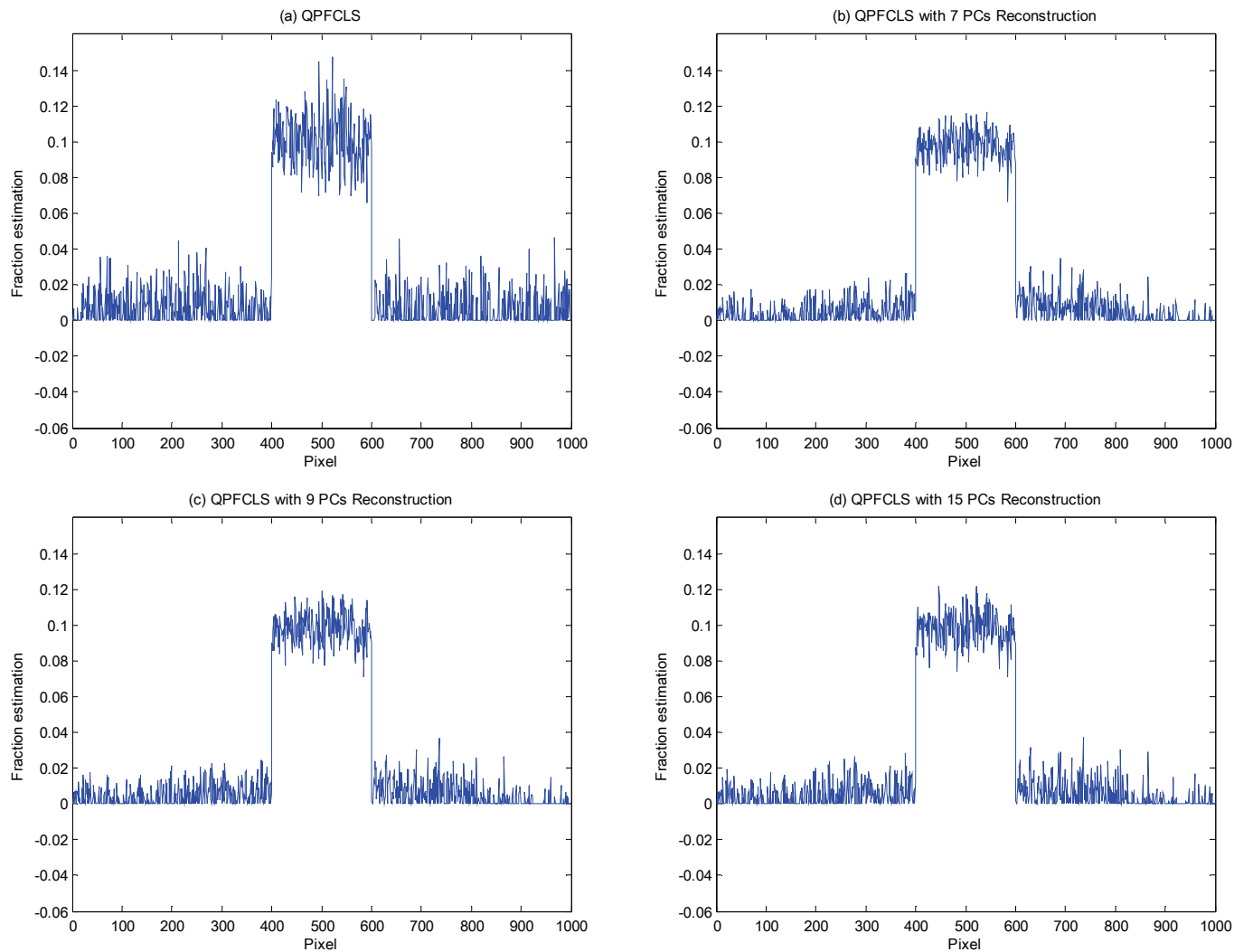


Figure 10: Estimation Results of (a) QPFCLS and QPFCLS with (b) 7, (c) 9, and (d) 15 PCs Reconstruction (SNR=10:1)

number as the noise level grows. In addition, including more PCs can only result in a minor decline in estimation capability, as already illustrated in this example.

Real Hyperspectral Image Experiments for Fully Constrained Least Squares

In this example, the QPFCLS algorithm implemented with noise reduction is applied to a real hyperspectral image scene collected by the AVIRIS sensor over Cuprite, NV, USA, in 1997, which is available at <http://aviris.jpl.nasa.gov/html/aviris.freedata.html>. This image set was atmospherically corrected using the MODTRAN radiative transfer model at the Jet Propulsion Laboratory [25]. Our study is based on a subimage of this scene with 350×350 pixels and 224 spectral bands, shown in Figure 11. Due to water absorption and low SNR, bands 1–3, 105–115, and 150–170 have been removed. Since no previous knowledge about this scene is available, a preprocessing step is needed to determine the endmember spectra

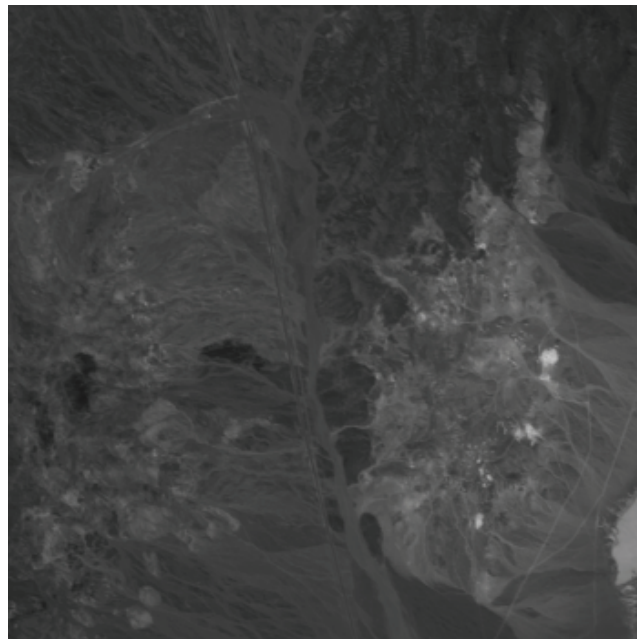


Figure 11: Spectral Band 30 of a Subimage of the AVIRIS Cuprite Image Scene

prior to the operation of our method. The same Neyman-Pearson detection theory-based method [24] used in the previous example is implemented here to estimate the number of the endmembers. A false-alarm probability of 10^{-4} leads to an estimation of 22 distinct endmembers. Then a simplex growing method [26] suggested by Chang *et al.* is adopted in this example to extract these 22 endmember spectral signatures. The spatial locations of the 22 endmembers generated by this method are shown in Figure 12, with the numbers indicating the order that the target endmembers are found. The fraction images

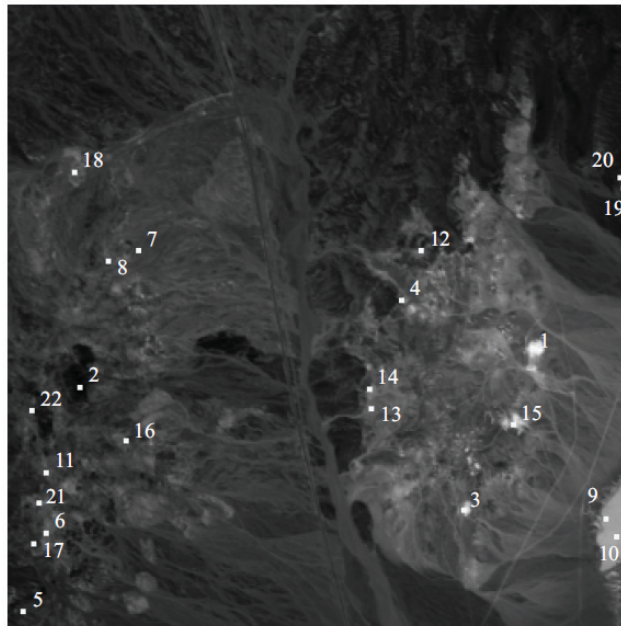
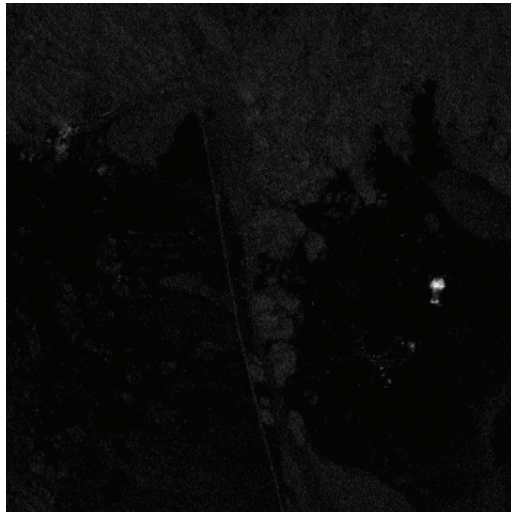


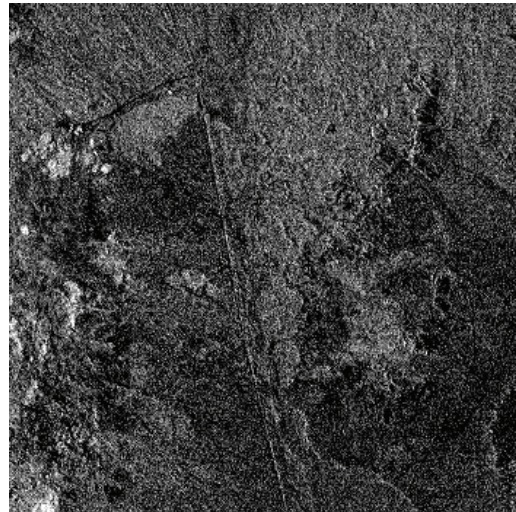
Figure 12: Spatial Locations of 22 Endmembers

obtained by the OSP and QPFCLS with noise reduction are displayed in Figures 13 and 14, respectively. Unlike computer simulations, we have no access to the ground truth of the image scene, which makes it difficult to directly evaluate the methods. However, although rigid proof is lacking that the QPFCLS with noise reduction produces better results than the OSP, it can be observed that the noise in the fraction images obtained by

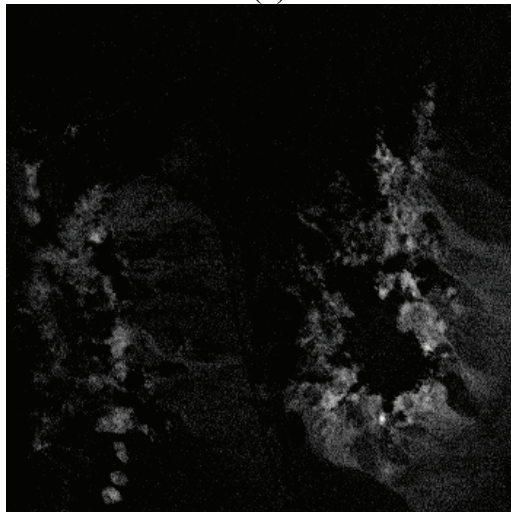
the former is less pronounced than that in the fraction images generated by the latter. Figure 13(b), 13(g), 13(j), 13(m), 13(s), and 13(t), for example, suffer from intense fluctuations of brightness, but their counterparts in Figure 14 are less subject to this problem. This improvement is consistent with what has been found in the previous computer simulations. Moreover, endmember abundance fractions should be continuous. The fractions obtained by the QPFCLS with noise reduction vary more smoothly in spatial spaces. Figure 14(c), 14(g), 14(h), 14(n) and 14(t), for example, have smoother transition than their counterparts in Figure 13.



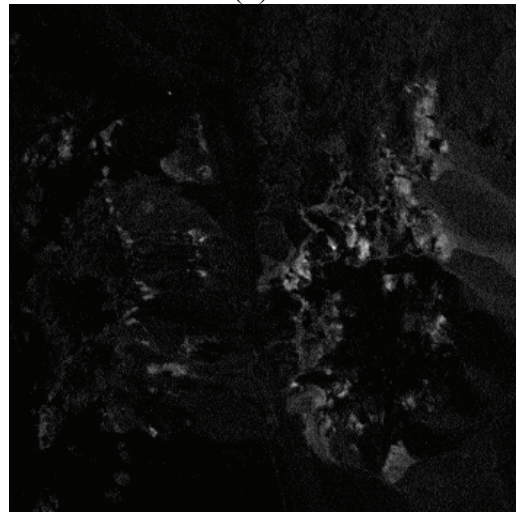
(a)



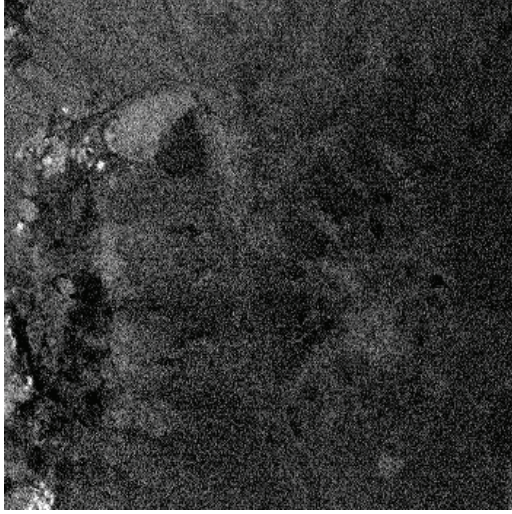
(b)



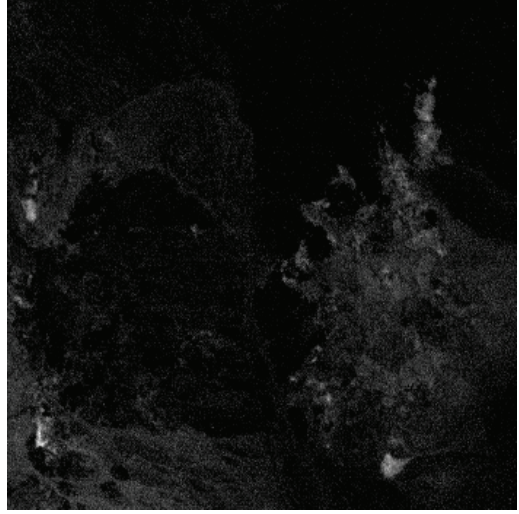
(c)



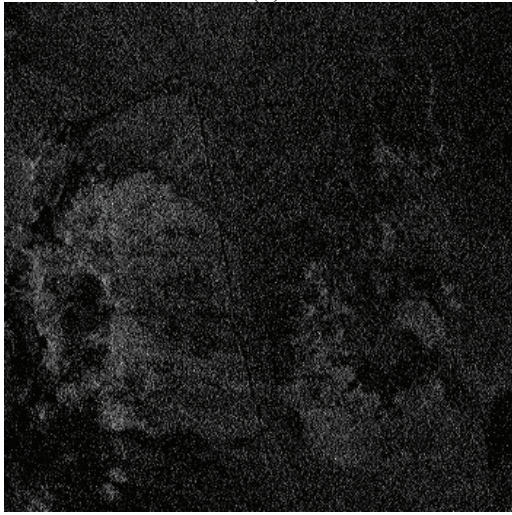
(d)



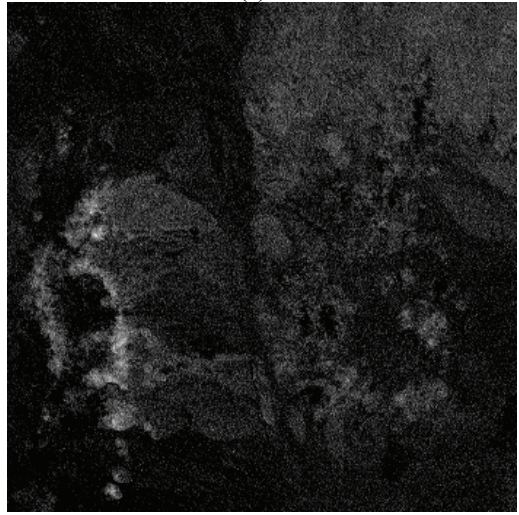
(e)



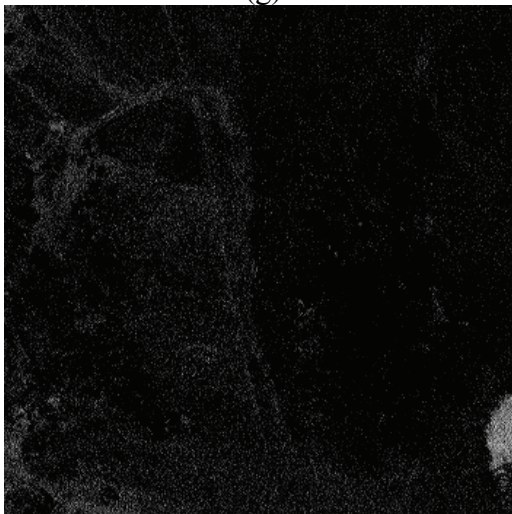
(f)



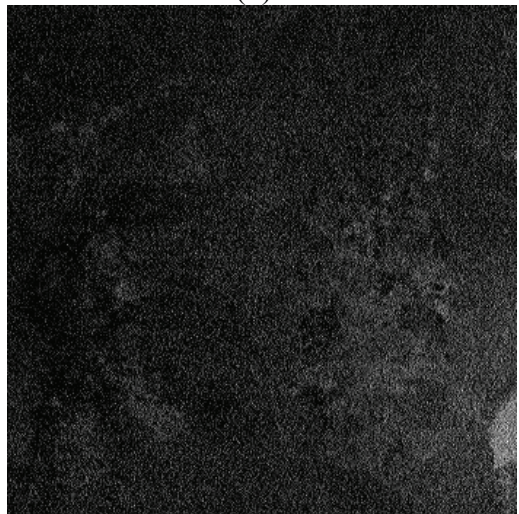
(g)



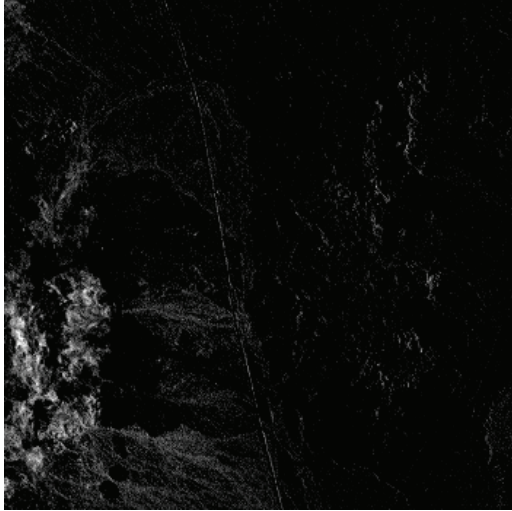
(h)



(i)



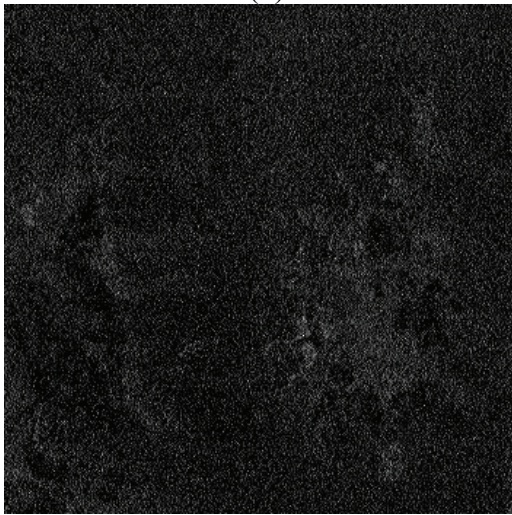
(j)



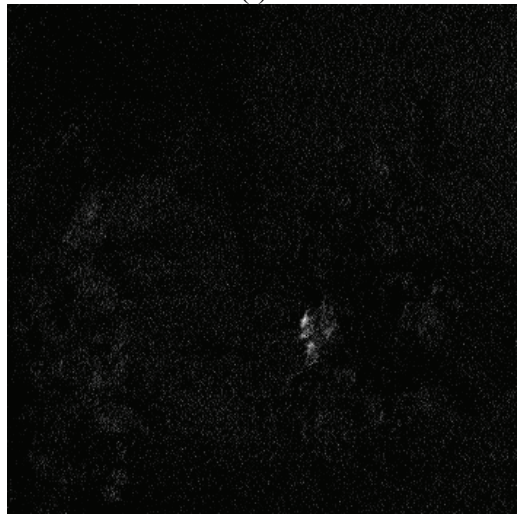
(k)



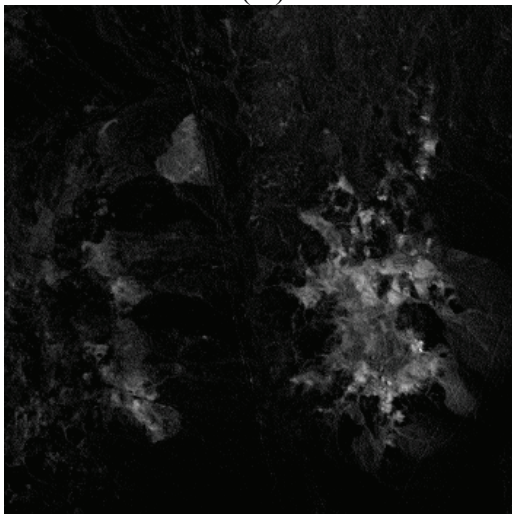
(l)



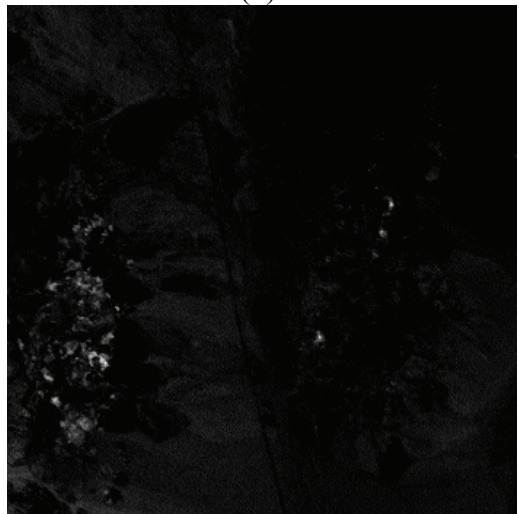
(m)



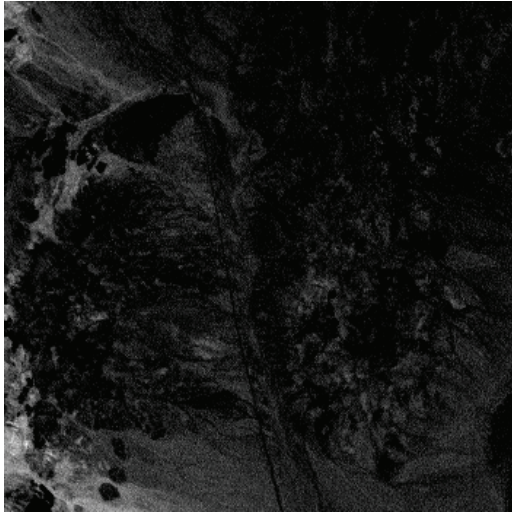
(n)



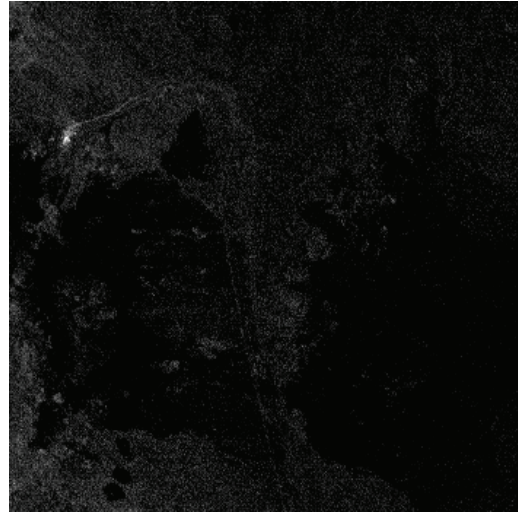
(o)



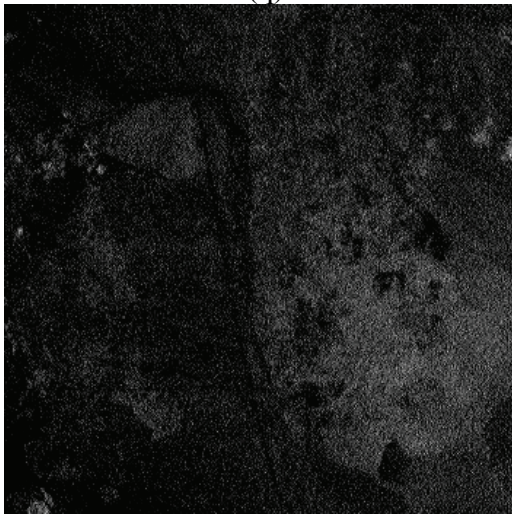
(p)



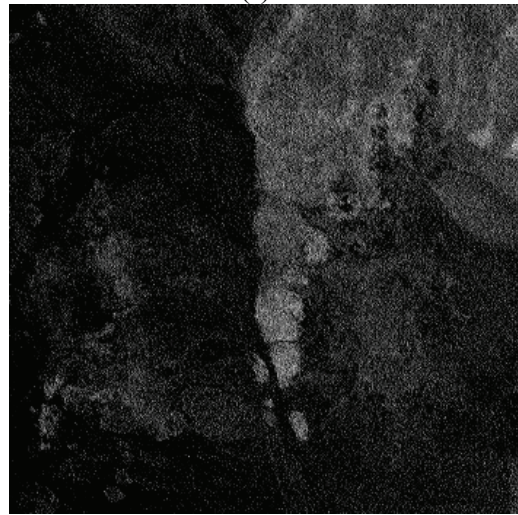
(q)



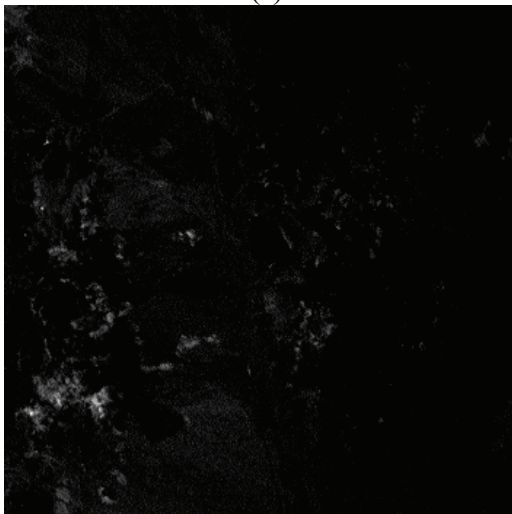
(r)



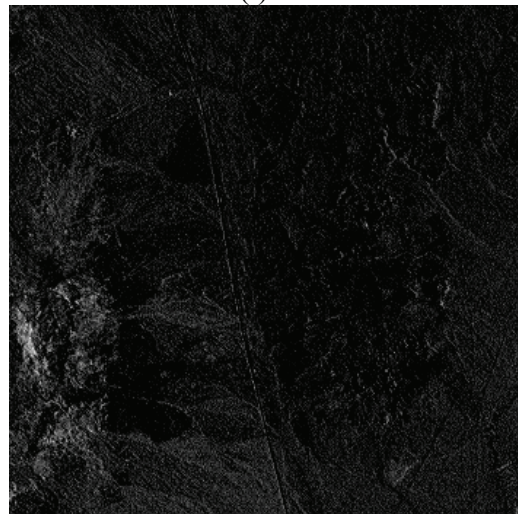
(s)



(t)

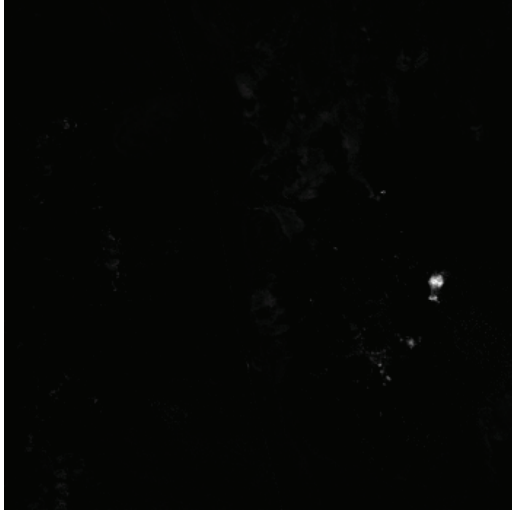


(u)



(v)

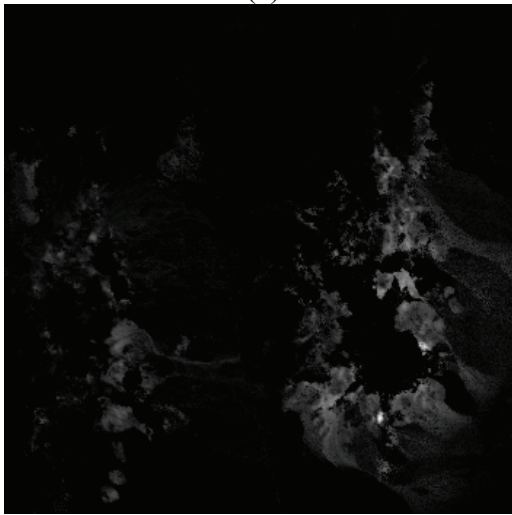
Figure 13: 22 Fraction Images Obtained by OSP



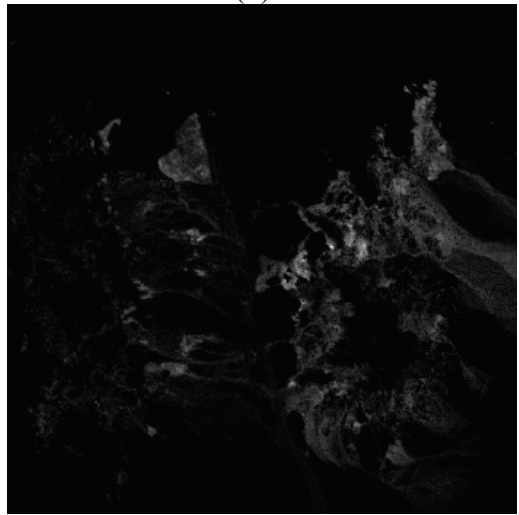
(a)



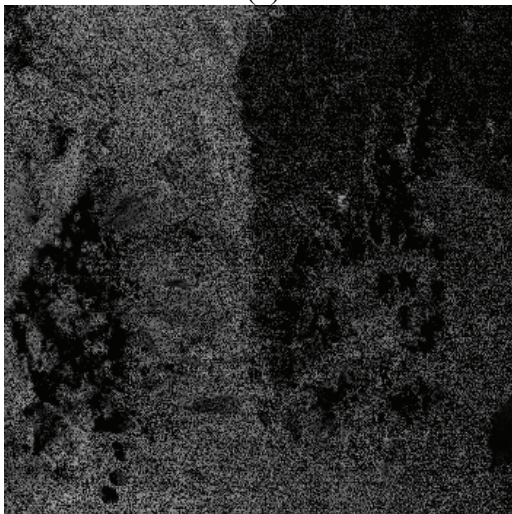
(b)



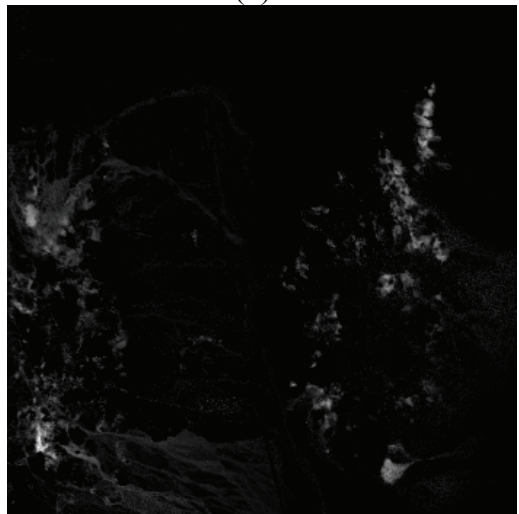
(c)



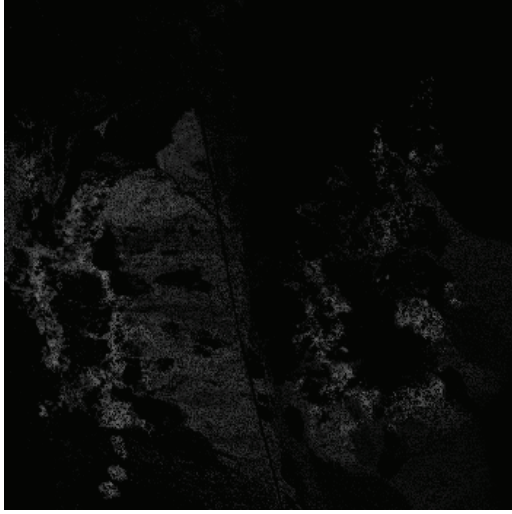
(d)



(e)



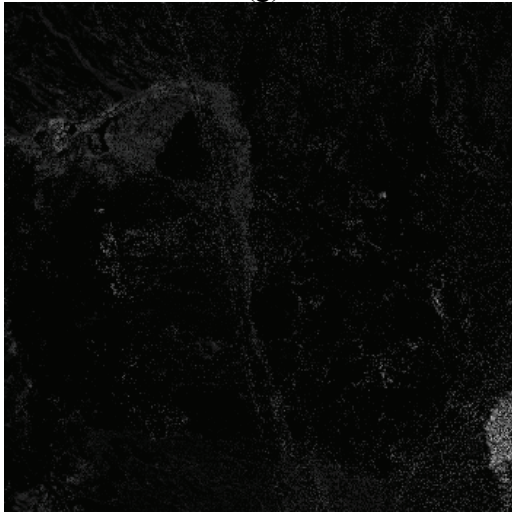
(f)



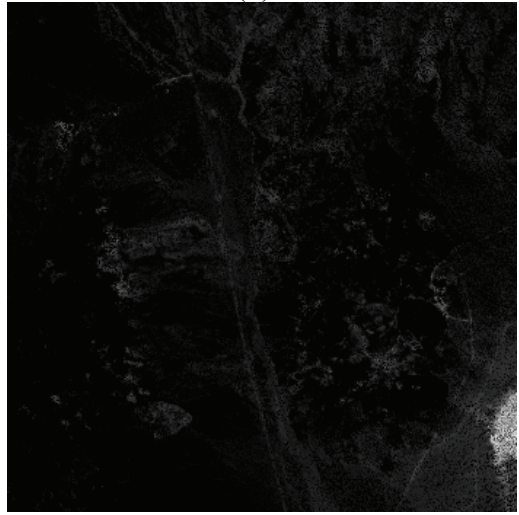
(g)



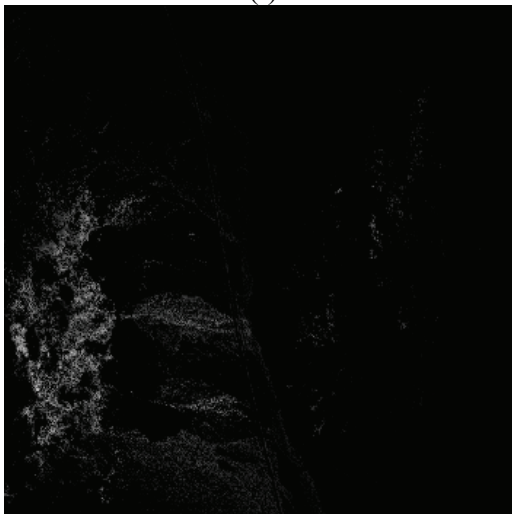
(h)



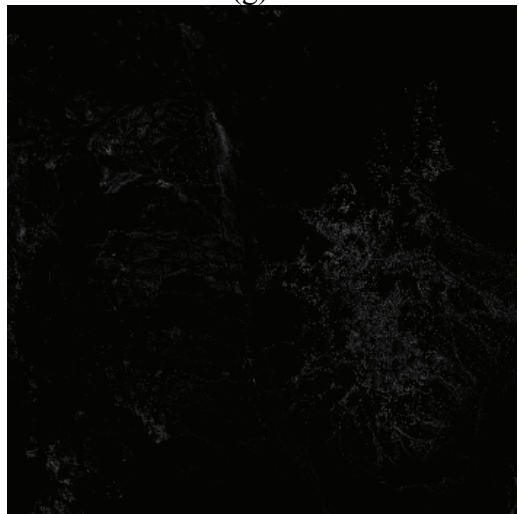
(i)



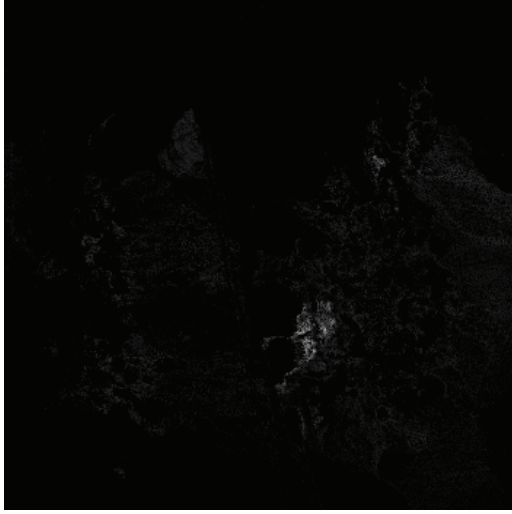
(g)



(k)



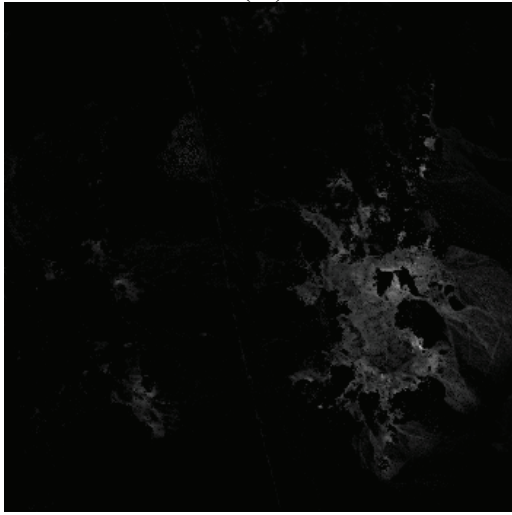
(l)



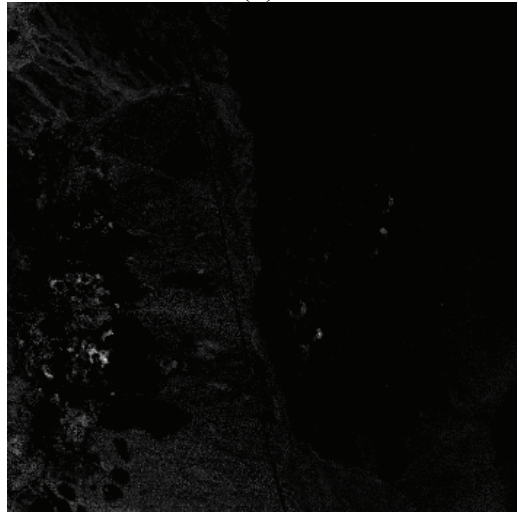
(m)



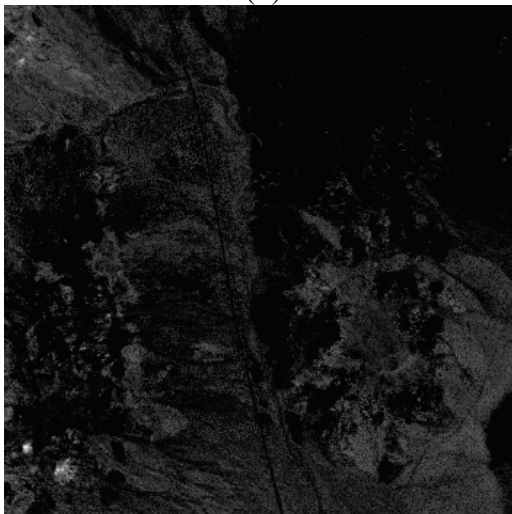
(n)



(o)



(p)



(q)



(r)

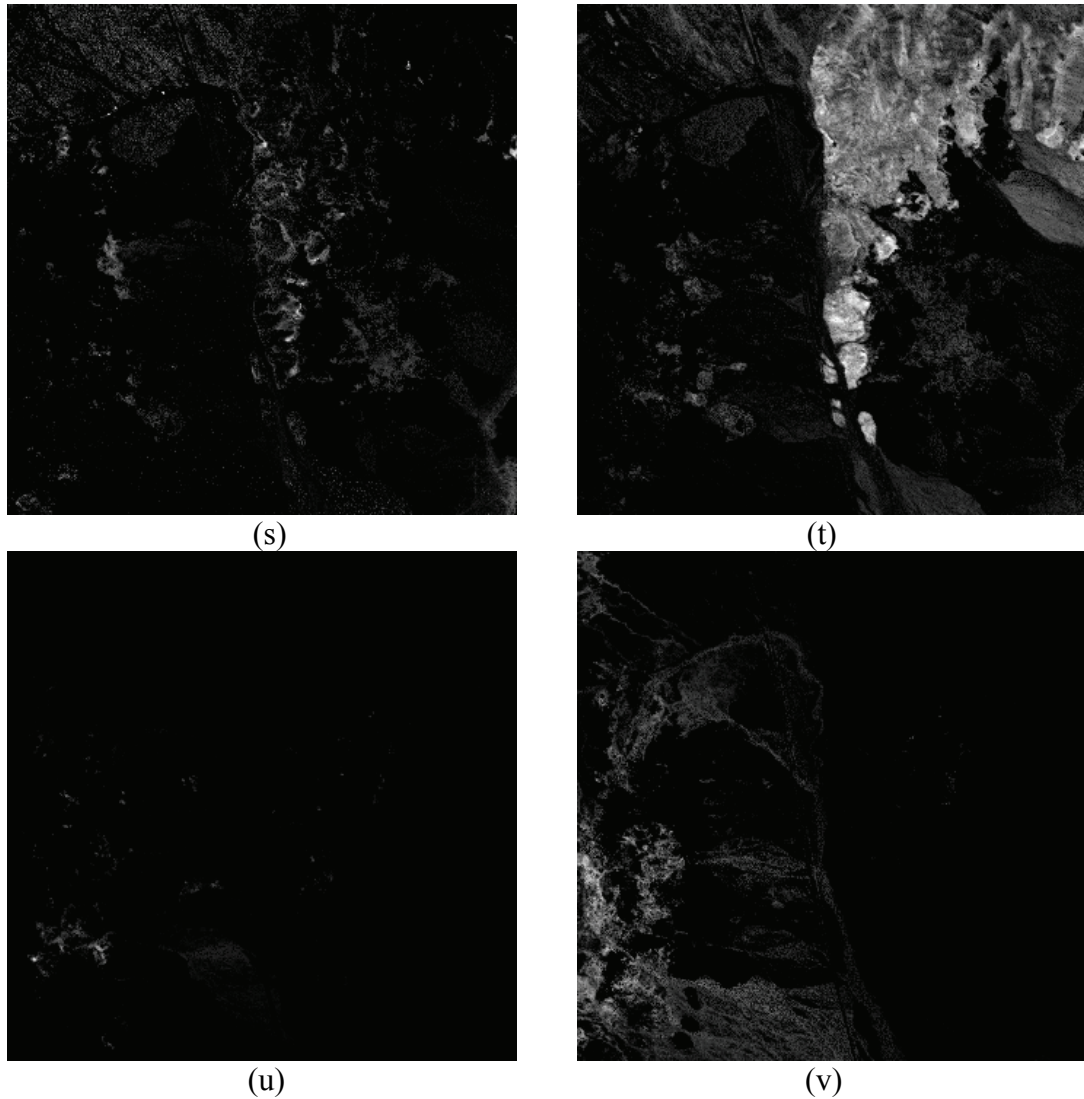


Figure 14: 22 Fraction Images Obtained by QPFCLS with Noise Reduction

Simulations for Unmixing with Nonnegativity and Relaxed Sum-to-One Constraints

In this section, we consider the situation where the sum-to-one condition is not strictly valid and demonstrate a comparative analysis among OSP [8], SCLS, QPFCLS, and R-QPFCLS. The first three approaches are selected to represent the unconstrained, partially constrained, and fully constrained approaches, respectively. The same set of

reflectance spectra and simulated fractions are used. The parameters for the implementation of the QPFCLS and R-QPFCLS are listed in Tables 1 and 5, respectively.

Table 5: Parameters for R-QPFCLS

t	$\alpha^{(1)}$	μ	ε	ε_{Newton}	l	h
1000	Equal Fractions	50	10^{-5}	10^{-4}	0.9	1.1

Sum-to-One Condition Strictly Satisfied

In this example, we demonstrate the performance of the R-QPFCLS using the nonnegativity and relaxed sum-to-one constraints when the sum-to-one condition is met. The sum of the fractions in each pixel is set to one to comply strictly with the sum-to-one condition. White Gaussian noise is added to every spectral band to achieve the SNR of 30:1. Figure 15 displays the fraction estimations of saltbrush, which is added only to pixel numbers 400–600 with 10% fraction. The RMS errors are 5.229×10^{-3} for OSP, 5.182×10^{-3} for SCLS, 3.956×10^{-3} for QPFCLS, and 3.970×10^{-3} for R-QPFCLS. We find that the QPFCLS produces the best estimate when the sum-to-one condition is strictly satisfied. However, relaxing the sum-to-one constraint does not significantly sacrifice the performance of the R-QPFCLS. The RMS errors of all seven materials are listed in Table 6. However, this will not be the case as we add variations to the fraction vectors.

Sum-to-One Condition Not Satisfied

In this example, we simulate the situation where the sum-to-one condition is not satisfied by multiplying each fraction vector by a random variable \mathbf{x} , where

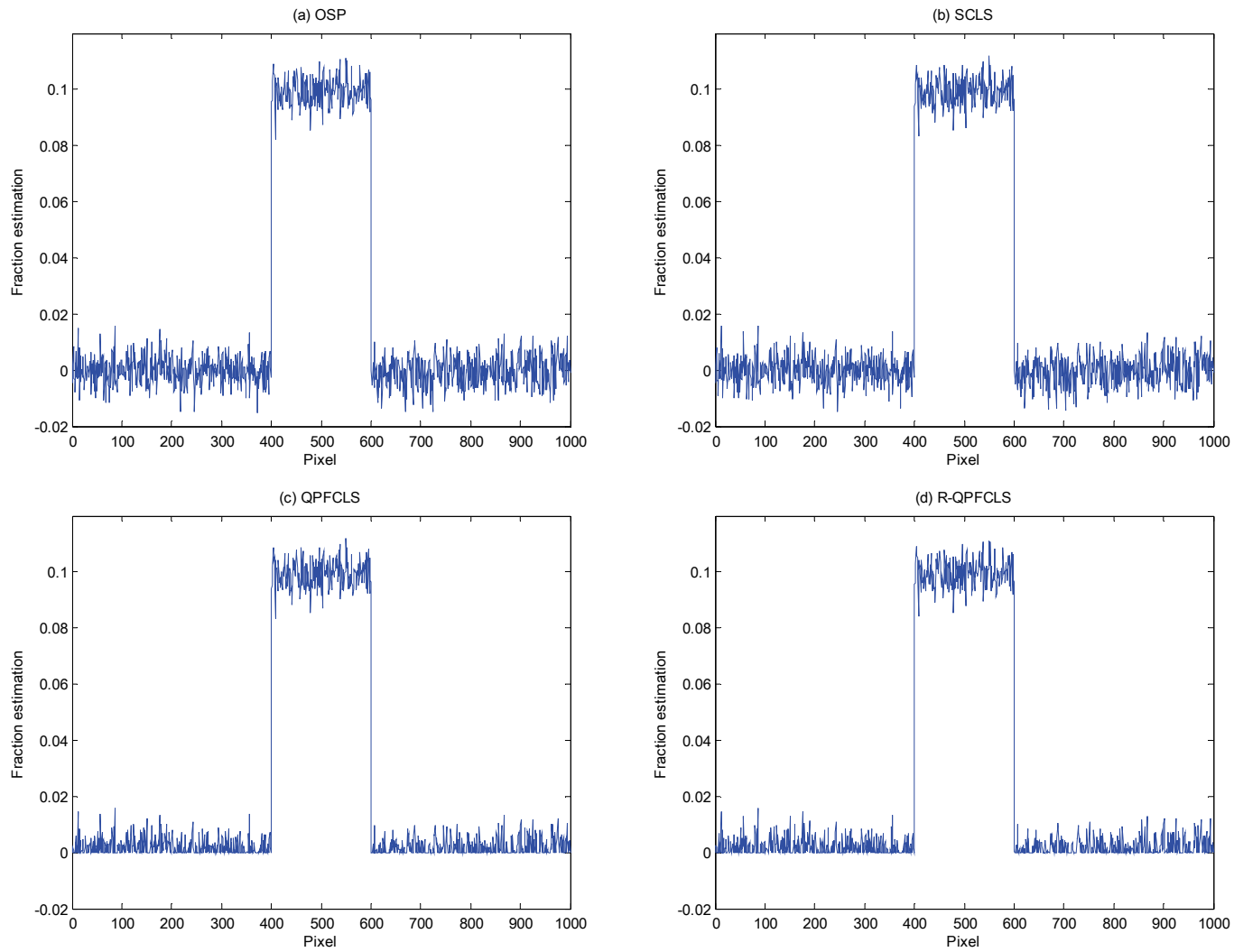


Figure 15: Estimation Results of (a) OSP, (b) SCLS, (c) QPFCLS, and (d) R-QPFCLS When Sum-to-One Condition Satisfied

Table 6: Root Mean Square Errors of Seven Materials
When Sum-to-One Condition Satisfied

Endmember	OSP	SCLS	QPFCLS	R-QPFCLS
Maple leaf	1.486×10^{-2}	7.599×10^{-3}	6.378×10^{-3}	1.304×10^{-2}
Blackbrush	2.690×10^{-2}	2.414×10^{-2}	2.242×10^{-2}	2.423×10^{-2}
Pinon pine	2.992×10^{-2}	2.889×10^{-2}	2.647×10^{-2}	2.712×10^{-2}
Aspen leaf	1.985×10^{-2}	1.378×10^{-2}	1.295×10^{-2}	1.795×10^{-2}
Saltbrush	5.229×10^{-3}	5.182×10^{-3}	3.956×10^{-3}	3.970×10^{-3}
Azurite	4.382×10^{-3}	3.905×10^{-3}	3.534×10^{-3}	4.292×10^{-3}
Sagebrush	5.709×10^{-3}	5.700×10^{-3}	4.648×10^{-3}	4.777×10^{-3}

$\mathbf{x} \sim N(\mu, \sigma^2)$. We set the values μ and σ to be 1 and 0.0304, respectively. The fraction vector that we need to estimate in each pixel becomes $\alpha_{New} = \mathbf{x}\alpha$. Estimation results of saltbrush are illustrated in Figure 16. We find that the QPFCLS, a method specifically designed to handle both the sum-to-one and nonnegativity constraints, degrades the most when the sum-to-one condition is not met. The RMS errors are 5.439×10^{-3} for OSP, 6.809×10^{-3} for SCLS, 9.754×10^{-3} for QPFCLS, and 4.239×10^{-3} for R-QPFCLS. The RMS errors of all seven materials are given in Table 7. Apparently, the QPFCLS, a fully constrained approach is less effective than the R-QPFCLS in handling the situation where the sum-to-one condition is not satisfied.

Table 7: Root Mean Square Errors of Seven Materials
When Sum-to-One Condition Not Satisfied

Endmember	OSP	SCLS	QPFCLS	R-QPFCLS
Maple leaf	1.500×10^{-2}	6.108×10^{-2}	4.821×10^{-2}	1.285×10^{-2}
Blackbrush	2.644×10^{-2}	6.283×10^{-2}	4.496×10^{-2}	2.335×10^{-2}
Pinon pine	2.887×10^{-2}	4.686×10^{-2}	3.472×10^{-2}	2.574×10^{-2}
Aspen leaf	1.984×10^{-2}	6.816×10^{-2}	5.383×10^{-2}	1.749×10^{-2}
Saltbrush	5.439×10^{-3}	6.809×10^{-3}	9.754×10^{-3}	4.239×10^{-3}
Azurite	4.232×10^{-3}	1.003×10^{-2}	2.198×10^{-2}	4.030×10^{-3}
Sagebrush	5.951×10^{-3}	6.012×10^{-3}	1.801×10^{-2}	4.956×10^{-3}

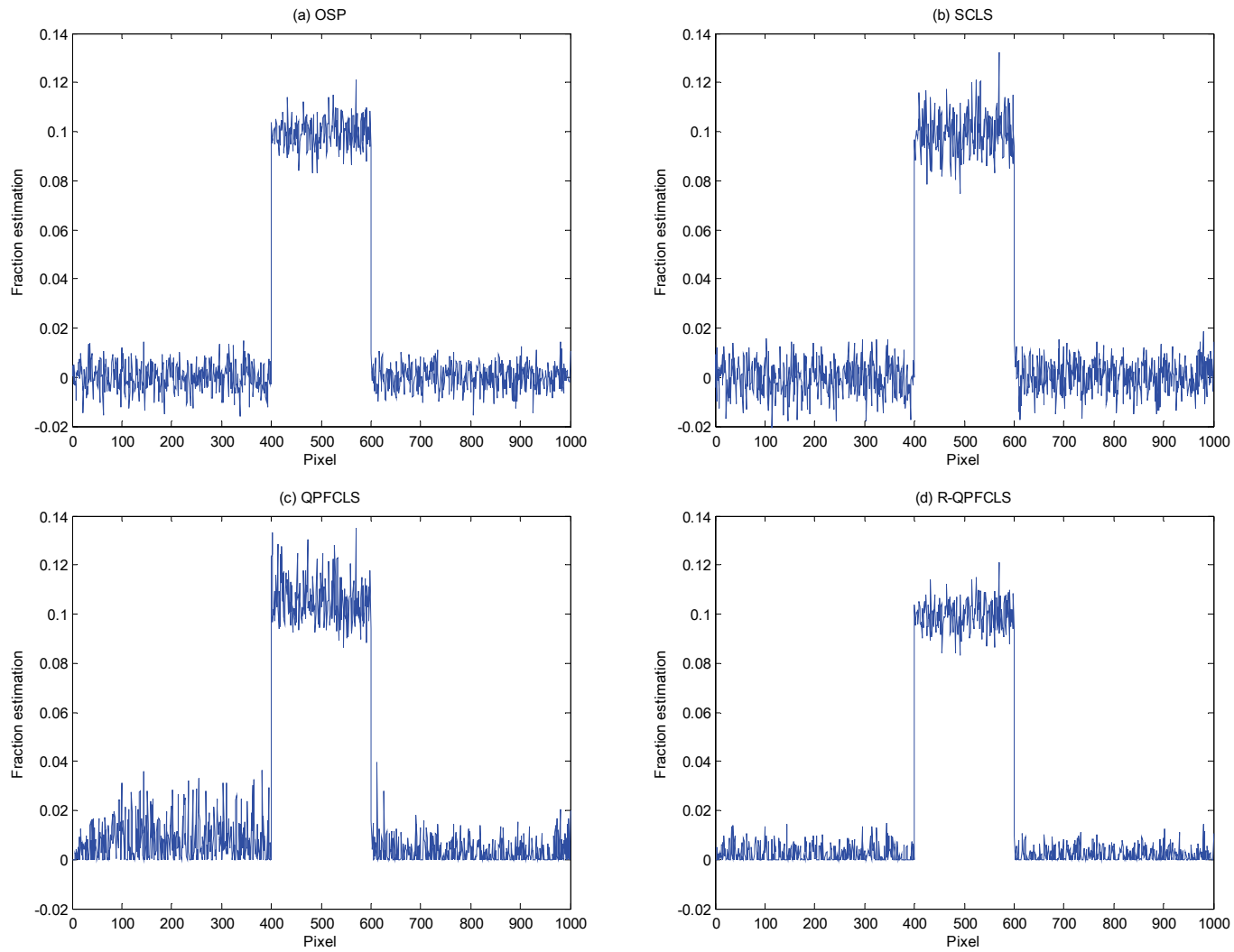


Figure 16: Estimation Results of (a) OSP, (b) SCLS, (c) QPFCLS, and (d) R-QPFCLS When Sum-to-One Condition Not Satisfied

CHAPTER FIVE

Conclusion and Future Work

Conclusion

When the size of the targets of interest is smaller than the hyperspectral image resolution, the need arises to estimate the endmember fractions. Two estimation methods are presented in this paper. The first method considers both the sum-to-one and nonnegativity constraints when developing a new fully constrained least squares estimation. We also use the noise-adjusted principal components transform to reduce the noise in hyperspectral images, which extends the capability of this estimation method. Experiments with simulated data and real AVIRIS image data demonstrate that our fully constrained method, the QPFCLS, can generate results comparable to those obtained by an existing linear unmixing method, the FCLSLU, and superior to the OSP and sum-to-one constrained least squares estimation and that noise reduction can significantly enhance the performance of our approach when the noise level rises.

The first proposed method relies on the validity of the linear mixture model. Nevertheless, the linear mixture model is strictly valid for the situation where the endmembers are arranged on the surface in a segregated manner. If, however, the endmembers are in a more intimate association, the suggested method may become less accurate as the linear mixture model does not remain valid. To circumvent this difficulty, we propose the relaxed sum-to-one constraint and the second unmixing method, R-QPFCLS. The unmixing with the nonnegativity and relaxed sum-to-one constraints

provides more robust estimation of the abundance fractions when the sum-to-one constraint is violated, while producing similar results to other existing methods when the constraint holds.

Future Work

For computer simulations in this work, it is assumed that the endmember spectra are known *a priori*. For real hyperspectral image examples, a simplex growing method suggested by Chang *et al.* [26] is used to find the endmember spectra. The simplex growing method is based on the fact that a data cloud, created by the linear model together with the sum-to-one and nonnegativity constraints, forms a simplex. Thus, the entire hyperspectral pixel vectors in a scene should lie in a simplex, and the vertices of this simplex are the spectra of the endmembers present in the scene. The method proposed in [26] extracts endmember spectra directly from a hyperspectral image by finding a simplex that best fits the data cloud of the hyperspectral pixel vectors. However, the success of this method relies on the linear model and two physical constraints. The suggested future work of this research is to use the technology of clustering, especially clustering methods for high-dimensional problems, to develop a more robust method to find endmember spectra.

BIBLIOGRAPHY

- [1] Asher Space Research Institute,
http://asri.technion.ac.il/new_site_php/research_projects/hyperspectral/index.php.
- [2] S. Jia and Y. Qian, "Constrained nonnegative matrix factorization for hyperspectral unmixing," *IEEE Trans. Geosci. Remote Sensing*, vol. 47, no. 1, pp. 161–173, Jan. 2009.
- [3] J. B. Lee, A. S. Woodyatt, and M. Berman, "Enhancement of high spectral resolution remote sensing data by a noise-adjusted principal components transform," *IEEE Trans. Geosci. Remote Sensing*, vol. 28, no. 3, pp. 295–304, May 1990.
- [4] R. B. Singer and T. B. McCord, "Mars: Large scale mixing of bright and dark surface materials and implications for analysis of spectral reflectance," in *Proc. 10th Lunar Planetary Science Conf.*, New York, 1979, pp. 1835–1848.
- [5] B. Hapke, "Bidirection reflectance spectroscopy. I. theory," *J. Geophys. Res.*, vol. 86, no. B4, pp. 3039–3054, Apr. 1981.
- [6] J. W. V. Miller, J. B. Farison, and Y. Shin, "Spatially invariant image sequences," *IEEE Trans. Image Process.*, vol. 1, no. 2, pp. 148–161, Apr. 1992.
- [7] J. C. Harsanyi and C. I. Chang, "Hyperspectral image classification and dimensionality reduction: An orthogonal subspace projection approach," *IEEE Trans. Geosci. Remote Sensing*, vol. 32, no. 4, pp. 779–785, Jul. 1994.
- [8] C. I. Chang, "Orthogonal subspace projection (OSP) revisited: A comprehensive study and analysis," *IEEE Trans. Geosci. Remote Sensing*, vol. 43, no. 3, pp. 502–518, Mar. 2005.
- [9] J. A. Richards and X. Jia, *Remote Sensing Digital Image Analysis*. New York: Springer-Verlag, 1999.
- [10] S. M. Kay, *Fundamentals of Statistical Signal Processing: Detection Theory*. Upper Saddle River, NJ: Prentice Hall, 1998.
- [11] Y. E. Shimabukuro and J. A. Smith, "The least-squares mixing models to generate fraction images derived from remote sensing multispectral data," *IEEE Trans. Geosci. Remote Sensing*, vol. 29, no. 1, pp. 16–20, Jan. 1991.

- [12] S. M. Kay, *Fundamentals of Statistical Signal Processing: Estimation Theory*. Upper Saddle River, NJ: Prentice Hall, 1993.
- [13] S. Johnson, "The constrained signal detector," *IEEE Trans. Geosci. Remote Sensing*, vol. 40, no. 6, pp. 1326–1337, Jun. 2002.
- [14] C. L. Lawson and R. J. Hanson, *Solving Least Squares Problems*. Englewood Cliffs, NJ: Prentice Hall, 1974.
- [15] C. I. Chang and D. Heinz, "Constrained subpixel target detection for remotely sensed images," *IEEE Trans. Geosci. Remote Sensing*, vol. 38, no. 3, pp. 1144–1159, May 2000.
- [16] C. Kwan, B. Ayhan, G. Chen, J. Wang, B. Ji, and C. I. Chang, "A novel approach for spectral unmixing, classification, and concentration estimation of chemical and biological agents," *IEEE Trans. Geosci. Remote Sensing*, vol. 44, no. 2, pp. 409–419, Feb. 2006.
- [17] C. I. Chang, H. Ren, C. C. Chang, F. D'Amico, and J. O. Jensen, "Estimation of subpixel target size for remotely sensed imagery," *IEEE Trans. Geosci. Remote Sensing*, vol. 42, no. 6, pp. 1309–1320, Jun. 2004.
- [18] K. H. Haskell and R. J. Hanson, "An algorithm for linear least squares problems with equality and nonnegativity constraints generalized," *Math. Prog.*, vol. 21, no. 1, pp. 98–118, Dec. 1981.
- [19] S. Boyd and L. Vandenberghe, *Convex Optimization*. Cambridge, U.K.: Cambridge Univ. Press, 2004.
- [20] A. A. Green, M. Berman, P. Switzer, and M. D. Craig, "A transformation for ordering multispectral data in terms of image quality with implications for noise removal," *IEEE Trans. Geosci. Remote Sensing*, vol. 26, no. 1, pp. 65–74, Jan. 1988.
- [21] R. E. Roger, "Principal components transform with simple, automatic noise adjustment," *Int. J. Remote Sensing*, vol. 17, no. 14, pp. 2719–2727, Sep. 1996.
- [22] N. Keshava and J. F. Mustard, "Spectral unmixing," *IEEE Signal Process. Mag.*, vol. 19, no. 1, pp. 44–57, Jan. 2002.
- [23] R. N. Clark, G.A. Swayze, R. Wise, E. Livo, T. Hoefen, R. Kokaly, and S. J. Sutley, USGS digital spectral library splib06a: U.S. Geological Survey, Digital Data Series 231, 2007. Available online at: <http://speclab.cr.usgs.gov/spectral.lib06> (accessed 2 July 2009).
- [24] C. I. Chang and Q. Du, "Estimation of number of spectrally distinct signal sources in hyperspectral imagery," *IEEE Trans. Geosci. Remote Sensing*, vol. 42, no. 3, pp. 608–619, Mar. 2004.

- [25] A. M. Filippi and R. Archibald, "Support vector machine-based endmember extraction," *IEEE Trans. Geosci. Remote Sensing*, vol. 47, no. 3, pp. 771–791, Mar. 2009.
- [26] C. I. Chang, C. C. Wu, W. M. Liu, and Y. C. Ouyang, "A new growing method for simplex-based endmember extraction algorithm," *IEEE Trans. Geosci. Remote Sensing*, vol. 44, no. 10, pp. 2804–2819, Oct. 2006.